FEEDBACK CONTROL OF INDUSTRIAL SOLUTION POLYMERIZATION OF ACRYLIC ACID USING NIR MEASUREMENTS

Othman[1], N., Egraz[2], J.B., Sau[2], J.M., Févotte[1], G.

[1]LAGEP, UMR CNRS Q5007, Université Lyon 1, 43 bld. Du 11 novembre 1918. 69100 Villeurbanne. FRANCE. [2] COATEX, ZI Lyon Nord. 69727 Genay. FRANCE

Abstract: In situ Near Infrared spectroscopy is used to monitor and control the concentration of monomer in solution polymerization processes. The Partial Least Square optimization technique is used to correlate the NIR spectrum with the concentrations of monomer and polymer in the reactor. Non linear input-output linearizing geometric control is then designed to control the concentration of monomer in the reactor. Controlling the concentration of monomer has a direct influence on the product quality and is very important to ensure the process safety. The control strategy is validated on-line during the solution polymerization of acrylic acid in an industrial pilot-scale reactor.

Keywords: Chemical Industry, Batch Processes, Polymerization, Sensors, Non Linear Systems, Observers, Industrial Control.

1. INTRODUCTION

Recently, NIR (Near InfraRed) spectroscopy has found a wide spread use in the monitoring of polymerization processes since it presents several significant advantages. First of all, the fibre optic probe inserted in an existing reactor is directly in contact with the reaction medium, which ensures rapid measurements, without requiring any sample preparation. In aggressive industrial environments, fibre optics allow the spectrometer to be placed far away from the reactor and ensure rapid and accurate data transmission. Furthermore, a set of characteristics of the reacting medium can be evaluated in-line from the NIR spectrum by developing calibration models that can be transferred easily to other instruments.

The quality of the results of the NIR analysis depends on a number of arguments. In order to ensure good results, the impact of the required properties in the selected NIR region must be important. Moreover, the off-line measurements used for the calibration must be accurate and reliable. Finally, the performance of the instrument and the mathematical treatment of the spectrum have to be adapted to the process.

Many applications of NIR spectroscopy in polymerization processes deal with the on-line monitoring of the concentration of monomer in reactors. Long et al. (1993) employed the NIR spectroscopy to estimate the conversion of styrene in solution polymerizations. On-line monitoring of the conversion of methyl methacrylate was studied by Chabot et al. (2000) and Aldridge et al. (1993) in emulsion polymerization systems.

NIR spectroscopy can also be used to estimate physical properties in real time. Gossen et al. (1993), applied the NIR spectroscopy to estimate the concentration of styrene and the particle size in an emulsion polymerization. Santos et al. (1998) used the NIR to estimate the particle size distribution in suspension polymerizations of styrene. They used the PLS (Partial Least Square) and Neural networks to correlate the absorbance with the particle size. These results allowed the authors to develop a technique for controlling the particle size distribution in a batch process (Santos et al., 2000).

In this work we are interested in controlling the concentration of acrylic acid in an industrial solution

polymerization reactor. In this case, the polymerization reaction is very fast and exothermic. Controlling the concentration of monomer is therefore essential to ensure the process safety through the mastery of the heat release of the reaction. Moreover, the concentration profile of the monomer in the reactor strongly influences the product quality – mainly the polymer molecular weight – during homopolymerization reactions, and the polymer composition during copolymerization processes so that suitable and reproducible concentration trajectories are required to ensure satisfactory and reproducible polymer properties.
In order to ensure such control, a calibration model based on the NIR spectra was developed and validated to estimate the concentrations of monomer and polymer in the reactor. The measurement strategy is presented in the first part of the paper. In a second part, an estimator of the reaction rate is designed which is necessary to apply closed loop control strategies. Finally, a non linear geometric approach is developed to control the concentration of monomer during the reaction.

2. NIR MEASUREMENT STRATEGY

2.1 Experimental setup

The polymerization process is carried out in a 30 L jacketed well mixed reactor equipped with internal reflux condenser. The stirrer is equipped with a Rushton turbine, the stirring rate being 150 rpm. The reactor is operated under semi batch conditions: four volumetric pumps are used to feed the reactor with solvent, homogeneous catalyst, radical initiator and monomer. The four corresponding flow rates can be controlled on-line through the measurement of the mass of reactants and the manipulation of the set point flow rates of the pumps. The reactants initially fed in the load of the reactor are first heated using the jacket. After the starting of the reaction, the fluid in the jacket is used as a coolant since the process is very exothermal. The main temperatures of the plant are measured using Pt100 Ω probes. The acquisition and storage of the measurements (Temperatures and flow rates) is performed using a first computer equipped with Labview®. The state observer and the control law described below, which use the NIR measurements of the concentration of acrylic acid, are computed and applied using the same computer. The NIR transmission probe is immersed in the reactor, it is connected through fibre optics to a FOSS NIRSystems® industrial spectrometer; and the spectral data are acquired and processes by a second computer. Both computers are connected in order to exchange data.
With the process in question, the production of poly-acrylic acid is performed following a rather complex operating policy including various heating, feeding and curing periods. The overall processing time is of the order of 2 hours. For the sake of confidentiality, no more details will be given about the operating procedure.

2.2 In-line NIR measurements of the conversion of acrylic acid

The NIR spectrum reflects the energy absorbed or reflected by the molecules present in any chemical medium crossed by a NIR light beam. For any wavelength, the energy absorbed by the molecules depends on the chemical and physical nature of the constituents, on their concentrations and on the volume of transmission. Some energy is also partly reflected without absorbance.
The near infrared spectral region, which covers the range from 700 to 2500 nm, expresses much of the chemical and structural information on the reaction medium, but the information tends to be in broad and overlapped bands. The processing of NIR spectral data was shown to allow the real-time evaluation of key parameters such as monomer concentration(s) or potential fluctuations of the quality of raw materials or to evaluate more specific variables such as the acid value during polyester production, density and melt index of polyethylene, the average particle diameter during emulsion or suspension polymerization processes; or the polymer composition during extrusion processes. Due to the variety and the complexity of the NIR spectral data, it is necessary to use "black-box" and multivariate data-processing models in order to extract the criterion of interest among the whole of the information contained in the recorded spectra. The "parameters" of such models are computed from a calibration data set and should be validated thereafter. The success of further on-line predictions depends on various criteria: the sampling technique, the off-line measurement method which was used and finally, the processing algorithm applied to the spectrum in order to draw the appropriate criterion.
It appeared that the main time variations in the spectrum during the polymerization under investigation can be observed between 1600 and 1900 nm. Fig.1 shows the difference between the spectrum obtained at the beginning of a semi-continuous polymerization of acrylic acid and that obtained 2 hours later. A PLS model was developed to correlate the spectrum with off-line measurements of the concentrations of acrylic acid, obtained through HPLC (High Pressure Liquid Chromato-graphy) and of polyacrylic acid, obtained after heating the polymer solution at 140°C.

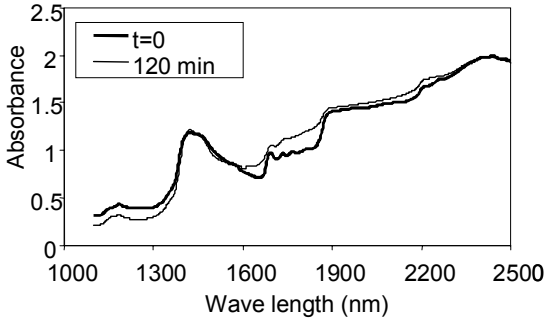

Fig. 1. NIR spectrum obtained at the beginning of a semi-continuous polymerization of acrylic acid and spectrum 2 hours later.

The "calibration model" was validated through the measurement of additional samples which were not taken into account during the calibration procedure. Fig. 2 displays the concentration values predicted using the calibration model against the calibration data set. Despite significant differences in the operating conditions involved during the acquisition of these data, the "measurements" appear to be rather reliable.

For validation purposes, NIR measurements were then performed during semi-batch and continuous polymerization reactions. Fig. 3 shows the in-line measurements obtained during the validation experiments.

The same calibration strategy was also applied to estimate the concentration of polymer in the reactor. In this case, the off-line calibration measurements were obtained through the gravimetric evaluation of the dry content. Figs. 3 and 4 display the validation results which were obtained, using the PLS model, during two polymerization operations. Samples were withdrawn from the reactor to assess the accuracy of the NIR estimates. As one can see, the in-line measurements of both acrylic acid concentration and polymer content were found to be really satisfactory.

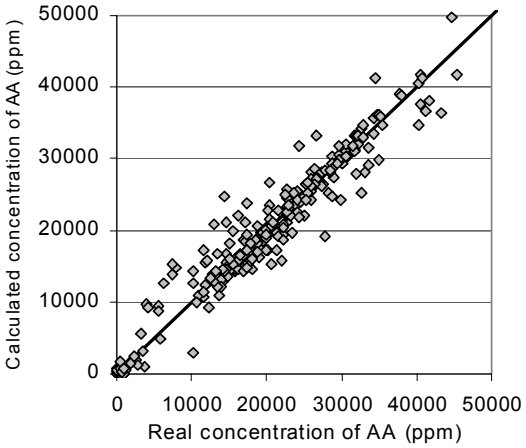

Fig. 2. Validation of the NIR calibration model. Estimation of the concentration of monomer during both semi-continuous and continuous reactions.

3. IN-LINE ESTIMATION OF THE POLYMERIZATION RATE

3.1 Simplified kinetic modeling of the polymerization reaction

The radical polymerization of acrylic acid is performed in aqueous solution. For the sake of confidentiality, the reactants which are used as co-solvents, catalyst and chain transfer agents will not be revealed in the present paper. The consumption of acrylic acid (AA) during the process can be described as follows:

$$\frac{dN_{AA}}{dt} = Q_{AA}^{in} - R_P = Q_{AA}^{in} - \underbrace{k_p[R^*]N_{AA}}_{propagation\ \ rate} \quad (1)$$

where N_{AA} is the number of moles of AA, Q_{AA}^{in} is the inlet molar flow rates of AA (mol/s), R_P is the reaction rate (mol/cm^3), k_p is the propagation rate constant (cm^3/mol/s), and $[R^*]$ is the concentration of radicals (mol/cm^3).

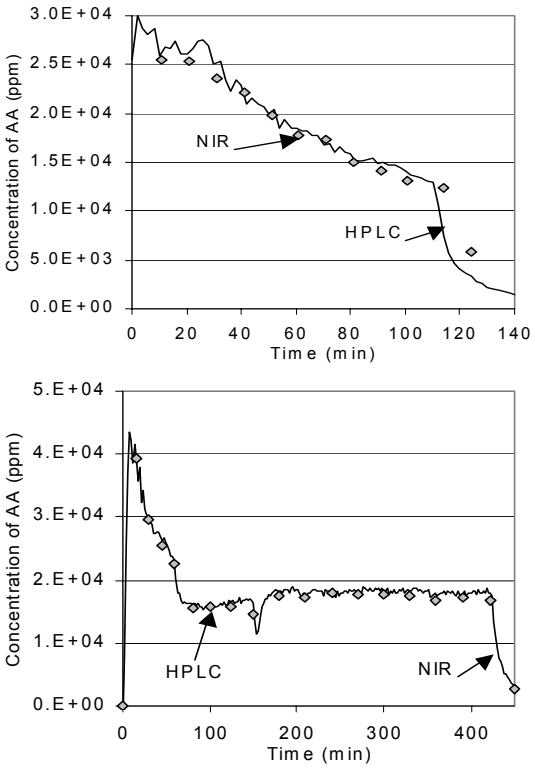

Fig. 3. Validation of the NIR calibration model: measurement of the concentration of monomer during both semi-continuous and continuous reactions.

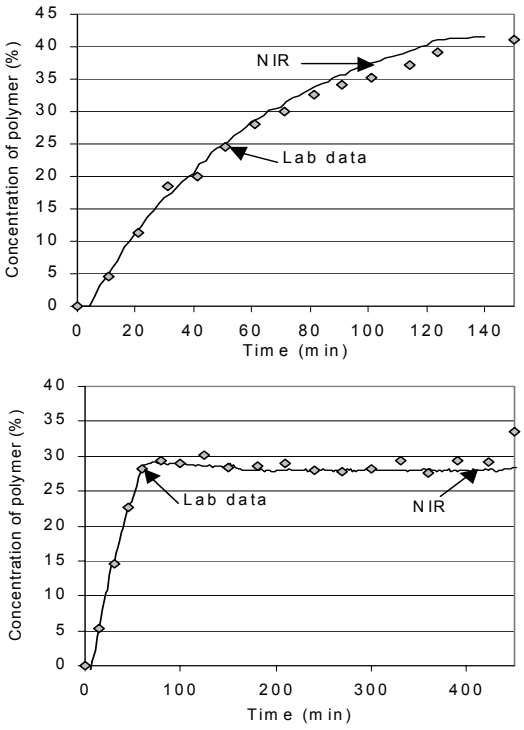

Fig. 4. Validation of the NIR calibration model: measurement of the polymer content during both semi-continuous and continuous reactions.

Expression (1) appears as a very simple, first order (with respect to AA), kinetic equation. However, whatever the reaction medium, it is well known that the polymerization in question is far from being simple as both the propagation rate constant and the concentration of radicals are likely to be significantly time varying, according to the concentration of reactants and products, complex pH variations and temperature.

For control purposes, and from an industrial point of view, it is not necessarily relevant to try a complex knowledge-based chemical modelling of the reacting system. Indeed, in the industrial context, efficient control can be designed without time-consuming and expensive theoretical studies. This is the reason why the reaction rate was estimated on-line, rather than predicted using any advanced model of the reaction.

3.2 A non linear high gain observer of the reaction rate of acrylic acid

The measurement of the concentration of monomer obtained by the NIR analysis allows us to estimate the reaction rate and, if the reaction rate constant is known, to estimate the concentration of radicals in the reactor [R^*]. In order to estimate the reaction rate of monomer, we set the following system where Rp is considered as a state variable with unknown dynamics:

$$\begin{bmatrix} \dot{N}_{AA} \\ \dot{R}_P \end{bmatrix} = \begin{bmatrix} Q_{AA}^{in} \\ 0 \end{bmatrix} + \underbrace{\begin{bmatrix} 1 & -1 \\ 0 & 0 \end{bmatrix}}_{A} \begin{bmatrix} N_{AA} \\ R_P \end{bmatrix} + \begin{bmatrix} 0 \\ \varepsilon \end{bmatrix} \quad (2)$$

ε represents the unknown dynamic of R_P.

A change of coordinates is required to put the system under a canonical form of observability. As the number of moles of acrylic acid is measured, we can use a high gain observer (see e.g., Farza et al., 1997, McKenna et al., 2000) to estimate the reaction rate as follows:

$$\begin{bmatrix} \dot{\hat{N}}_{AA} \\ \dot{\hat{R}}_P \end{bmatrix} = \begin{bmatrix} Q_{AA}^{in} \\ 0 \end{bmatrix} + \underbrace{\begin{bmatrix} 1 & -1 \\ 0 & 0 \end{bmatrix}}_{A} \begin{bmatrix} N_{AA} \\ \hat{R}_P \end{bmatrix} - \begin{bmatrix} 2\theta \\ \theta^2 \end{bmatrix} \left(\hat{N}_{AA} - N_{AA} \right) \quad (3)$$

The rate of convergence of the observer is very easy to tune using the single positive parameter θ.
The estimation results are shown on Fig. 5 for a semi-continuous reaction. Due to the operating conditions involved, it appears that the reaction rate is equal to the flow rate of monomer. This means that the monomer inlet feed rate in the reactor can be increased to allow improved productivity: the reaction is so fast that there is no monomer accumulation during the reaction. Moreover, the propagation rate coefficient is constant since pH does not change during the reaction. Consequently, the concentration of radicals is found to be constant during all the reaction time.

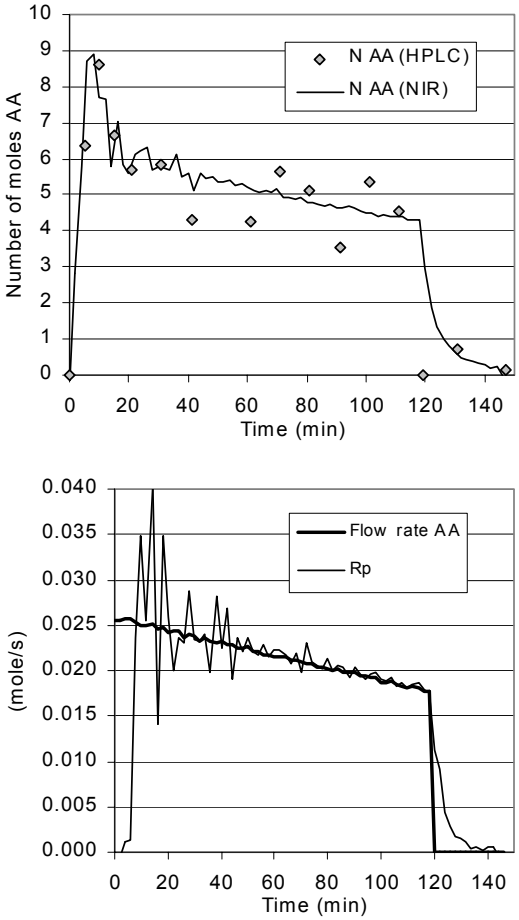

Fig. 5. State estimation of R_P in a semi-continuous reaction based on the on-line NIR measurement of the number of moles of acrylic acid, N_{AA}.

4. FEEDBACK CONTROL OF THE CONCENTRATION OF ACRYLIC ACID

Controlling the concentration of acrylic acid in the reactor allows us to maximize the process productivity by decreasing the reaction time while ensuring the process thermal safety. Actually, the polymerization of AA is very exothermic and fast. The amount of monomer in the reactor must therefore be calculated in a way that the cooling system remains able to evacuate the heat produced by the polymerization and allows to maintain the desired reaction temperature. Again, the amount of monomer in the reactor can be obtained using on-line NIR analysis and can be controlled by manipulating the inlet flow rate of monomer. The whole control system is schematically presented in Fig. 6.

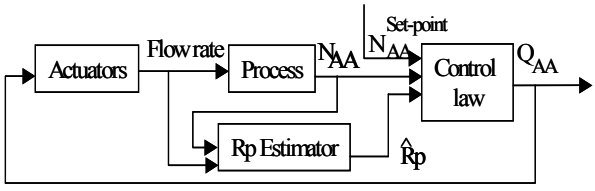

Fig. 6. Closed-loop system for the control of the monomer concentration during the semi-batch polymerization of acrylic acid, with state estimation of the polymerization rate Rp.

In order to design the controller, the following system is considered:

$$\begin{aligned} \dot{N}_{AA} &= Q_{AA}^{in} - R_P(N_{AA}) \\ y &= N_{AA} \end{aligned} \tag{4}$$

Since system (4) is nonlinear, a differential geometric nonlinear controller was designed in order to control N_{AA}. The adaptation of differential geometry for the analysis and design of nonlinear control systems was proposed by Herman and Krener (1977), Hunt et al. (1983) and Isidori (1989). The results generalize concepts and tools from linear control theory for a class of nonlinear systems, such as the state feedback.

The GLC framework is the calculation of a static-state feedback, under which the closed-loop I/O system is exactly linear. The state of the model need not to be transformed into linear one. Once the inner loop is closed, the controller design reduces to the design of an external linear controller with integral action.

The relative order, or the linearizability index r, of nonlinear systems can be calculated, as for linear systems, by calculating the derivative of the output. The relative order is the smallest order of derivative that depends explicitly on the input (Q_{AA}). For system (4), the relative order is equal to one. A geometric nonlinear input/ output linearizing control can therefore be constructed as given by the following system :

$$Q_{AA}^{in} = R_P + \kappa_p \underbrace{\left(N_{AA}^{set-point} - N_{AA}\right)}_{\varepsilon = error} \tag{5}$$

We notice that controlling N_{AA} requires the estimation of R_P that we obtain from the high gain observer.

A set of experiments with different set-points was performed in order to validate the controller robustness. During experiment 170 the set point varies smoothly. Fig. 7 shows that N_{AA} takes some time to converge to the desired value. This dynamic behaviour is mainly due to the fact that there is no monomer in the initial charge. The delay in the convergence can therefore be improved by introducing an amount of monomer in the initial charge. However, this can be critical during the heating phase, especially in an industrial reactor. On the other hand, the delay in convergence is amplified by the inhibition during the few first minutes of the reaction and the rapid change in the reaction rate when the reaction starts. Moreover, the convergence time is influenced by some inaccuracies of the NIR measurements, especially when the amount of monomer is small at the beginning of the reaction.

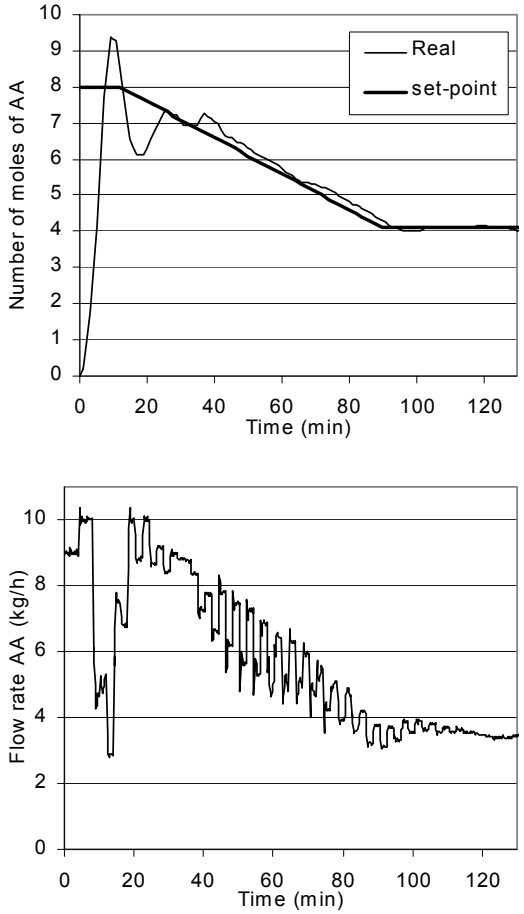

Fig. 7. Control of N_{AA} during experiment n°170. Tracking of trajectory for N_{AA}. The manipulated input is the inlet flow rate of AA.

In order to demonstrate that the convergence time is mainly due to physical limitations, and not to the controller itself, two experiments (referred to as run 173 and run 174 below) were performed with stiff changes in the set-point during the reaction. A step change of 1 and 1.5 moles are imposed during experiments 173 and 174, respectively. These experiments allowed us to assess the robustness of the controller under hard conditions even though such conditions are not supposed to occur during real industrial processing.

The obtained results are shown in Figs. 8 and 9.

From these figures, it can be observed that performances and closed-loop response of the controller are not the same at the beginning of the reaction compared with the rest of the polymerization process. The number of moles of acrylic acid N_{AA} converges more satisfactorily (i.e. fast convergence without oscillations) to the set-point during the reaction even with an important change in the set-point. This is due to the fact that once the reaction started, the reaction rate varies smoothly and allows the NIR measurements to be more precise.

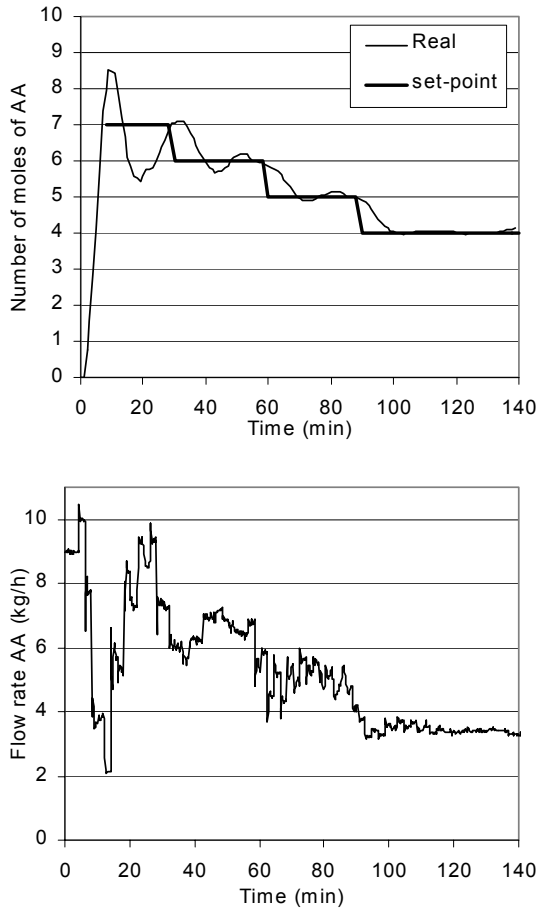

Fig. 8 Control of N_{AA} during Run 173: number of moles of AA and controlled flow rate of AA.

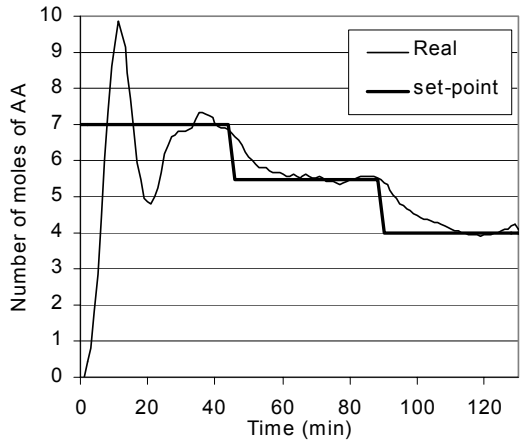

Fig. 8 Control of N_{AA} during Run 174: number of moles of AA and controlled flow rate of AA.

CONCLUSION

The control strategy developed in this work has been validated on an industrial pilot-scale reactor, taking into account real industrial constraints, in terms of aggressive environment and complex operating strategies). The control strategy gave good results even under hard conditions. In particular, it allowed to maintain the concentration of monomer in the reactor at a predefined value, which was calculated in such a way such the heat produced by the polymerization reaction did not affect the reaction temperature. Controlling the concentration of monomer in the reactor also allowed improving the mastery over the obtained polymer molecular weights, which is a key product property in this process. Such mastery, notably in terms of improved reproducibility, represents a major economical issue. It is worth noting that such application was made possible thanks to the availability of new in situ NIR sensors, which are certainly destined for numerous future industrial applications in the field of chemical processes.

REFERENCES

Aldridge, P., K.; J. J., Kelly; B. Callis. (1993) Noninvasive monitoring of bulk polymerization using short-wavelength near-infrared spectroscopy, *Analytical Chem.,* **65**, 381-3585.

Chabot, P, L., Hedli; Ch. Olmstead. (1993) On-line monitoring of emulsion polymerization, AT-Process, *J. Proc. Analytical Chem.*, **2000**, 1-6.

Farza, M., H., Hammouri, S., Othman , K., Busawon (1997) Nonlinear Observers for Parameter Estimation in Bioprocesses. Chem. Eng. Sci., **23**, 52, 4251-4267.

Gossen, P.D., J.F., MacGregor; R.H.,,Pelton (1993) Composition and particle diameter for styrene/ methyl methacrylate copolymer latex using UV and NIR spectroscopy, *Applied spectroscopy*, **47**, 11.

Herman, R. and A., Krener. (1977) Nonlinear controllability and observability, *IEEE Trans. Aut. Cont.*, AC-22, 5.

Hunt, R., Su, G., Meyer. (1983) Global transformations of nonliner systems, *IEEE Trans. Aut. Cont.*, 1983, AC-28, 24-31.

Isidori, A., (1989) Nonlinear control systems. An introduction (2nd Edition), Springer-Verlag, Berlin.

Long T.E., H.Y., B., Liu, A., Schell, D.M., Teegarden, D. S. Uerz. (1993) Determining of solution kinetics by NIR infrared spectroscopy. 1.Living anionic polymerization processes, *Macromolecules,* **26**, 6237-6242.

McKenna, T.F., S., Othman, G., Fevotte, A.M. Santos, H. Hammouri (2000) An integrated approach to polymer reaction engineering: a Review of Calorimetry and State Estimation. *Polym. React. Engng*, **8**, 1-38.

Santos, A.F., E.L., Lima, J.C., Pinto (1998) In-line evaluation of average particle size in styrene suspension polymerizations using near-infrared spectroscopy, *J. Appl. Polym. Sci*., **70**, 1737.

Santos, A.S., E.L., Lima, J.C., Pinto (2000) Control and Design of average particle size in styrene suspension polymerizations using NIRS, *J. Appl. Polym. Sci.*, **77**, 453-462.

DATA-DRIVEN MODELING OF BATCH PROCESSES

Dennis Bonné * **Sten Bay Jørgensen** *

* *Department of Chemical Engineering, Technical University of Denmark, DK-2800 Lyngby, Denmark, Email: (db or sbj)@kt.dtu.dk, Fax: +45 4593 2906*

Abstract: A one dimensional grid of interdependent linear models obtained from operation data is proposed for modeling repeated finite horizon, nonlinear and non-stationary process operations. Such finite horizon process operations include start-ups, grade transitions, shut-downs, and of course batch, semi-batch and periodic processes. The model grid is identified from data using a novel interpretation of generalized ridge regression that penalizes weighted discrepancies between one linear model and the models in its neighborhood. It is furthermore outlined how different representations of such a model grid may be used off-line as well as on-line, for prediction, monitoring, control, and optimization. Among these representations is a linear time-varying state space model which may be used for design in established linear monitoring and control methodologies.

Keywords: Batch, Non-linear systems, Time-varying systems, Parameter estimation

1. INTRODUCTION

Batch processes are experiencing a renaissance as products-on-demand and first-to-marked strategies impel the need for flexible and specialized production methods. Furthermore, industries such as food, biochemical, and pharmaceutical depend on the confinement of faults and contaminations to single batches. This renaissance propels the need for modeling and control tools, which can facilitate optimal and reliable operation of batch processes. However, the traditional linear modeling and control tools are inadequate, when applied to the often highly nonlinear and time-varying behavior of batch processes.

In section 2 it is thus proposed to model batch processes with a time-varying grid of linear models and it is demonstrated how such model grids may be applied to both off-line and on-line monitoring, prediction, control, and optimization. Identification of these model grids is addressed in section 3 and it is proposed to use model property based regularization to overcome excessive variance. The methods proposed in sections 2 and 3 are applied to an industrial case study in section 4 and finally conclusions are given.

2. TIME-VARYING MODELS

Most often the complex and nonlinear dynamics of continuously operated processes can be approximated with a moderate set of local Linear Time-Invariant (LTI) models, each of which describes a characteristic region in the operation window. These regions described by local models will often be characterized by a set of active constraints. For batch and semi-batch processes (from here on, batch will cover both batch and semi-batch processes) however, the set of active constraints will change as the batch progresses. In fact, to

operate a batch process in an optimal fashion, a specific sequence of constraints is tracked during operation. This means that local approximations of characteristic regions are not sufficient to describe batch operation. The transitions between these locally approximated characteristic regions are also needed to provide a complete description of batch operation. Furthermore, even if specific sets of constraints were active for longer periods; local LTI models can not be expected to describe the time variation due to changing holdups and/or compositions.

The periodic nature and the finite horizon of batch processes however, make it possible to model the evolution from each sample point to the next in a batch with one *grid-point* LTI model. In this fashion, both the time variation within the characteristic regions and the transitions between these may be approximated with a grid of grid-point models. Thus, such a model set gives a complete description of a batch. The finite horizon of batch processes means that the model set will be finite. The periodic way in which the same recipe is repeated batch after batch means that several measurements from the individual sample points are available for identification. That is, the time evolution of a process variable is measured/sampled at specific sample points during the batch operation and as the batch operation is repeated, several measurements are collected from every sample point. With multiple data points/measurements from one specific sample point a grid-point model can be identified for this sample point. Explicitly, in addition to the time dimension, data from batch processes also evolve in a batch index dimension.

2.1 Model Parameterization

Given the discussion above, batch processes are modeled with sets of dynamic grid-point LTI models. Such a set of grid-point LTI models could also be referred to as a Linear Time Varying (LTV) batch model. These grid-point LTI models can be parameterized in a number of ways – e.g. as Output Error (OE) models, AutoRegressive models with eXogenous inputs (ARX), State Space (SS) models, etc. In the present contribution the ARX model parameterization was chosen. This choice of parameterization offers a relatively good multivariable system description with a moderate number of model parameters.

As operation of a batch progresses, different inputs and outputs may be used depending on the current phase of the batch and hence in order to model batch operation it is convenient to define the following variables and references for each time step t: Input variable $u_t \in \mathbb{R}^{n_u(t)}$ with reference $\bar{u}_t \in \mathbb{R}^{n_u(t)}$, output variable $y_t \in \mathbb{R}^{n_y(t)}$ with reference $\bar{y}_t \in \mathbb{R}^{n_y(t)}$, and disturbance variable $w_t \in \mathbb{R}^{n_y(t)}$. Using an ARX model parameterization, the output deviation $\bar{y}_t - y_t$ at time t may be given as a weighted sum of $n_A(t)$ past output deviations and $n_B(t)$ past input deviations

$$\begin{aligned}\bar{y}_t - y_t = &- a_{t,t-1}\Big(\bar{y}_{t-1} - y_{t-1}\Big) - \dots \\ &- a_{t,t-n_A(t)}\Big(\bar{y}_{t-n_A(t)} - y_{t-n_A(t)}\Big) \\ &+ b_{t,t-1}\Big(\bar{u}_{t-1} - u_{t-1}\Big) + \dots \\ &+ b_{t,t-n_B(t)}\Big(\bar{u}_{t-n_B(t)} - u_{t-n_B(t)}\Big) \\ &+ w_t\end{aligned} \tag{1}$$

where $n_A(t), n_B(t) \in [1, \dots, t]$ are the grid-point ARX model orders and $a_{i,j} \in \mathbb{R}^{n_y(i),n_y(j)}$ and $b_{i,j} \in \mathbb{R}^{n_y(i),n_u(j)}$ are the grid-point ARX model parameter matrices. Note, as the grid points are modeled with individual grid-point models, the sample points t do not have to be equidistantly spaced in time. Let N be the batch length(/number of samples) and define the input $\boldsymbol{u}$, output $\boldsymbol{y}$, shifted output $\boldsymbol{y}^0$, and disturbance $\boldsymbol{w}$ profiles as

$$\begin{aligned}\boldsymbol{u} &= \begin{bmatrix} u_0' & u_1' & \dots & u_{N-1}' \end{bmatrix}' \\ \boldsymbol{y} &= \begin{bmatrix} y_1' & y_2' & \dots & y_N' \end{bmatrix}' \\ \boldsymbol{y}^0 &= \begin{bmatrix} y_0' & y_1' & \dots & y_{N-1}' \end{bmatrix}' \\ \boldsymbol{w} &= \begin{bmatrix} w_1' & w_2' & \dots & w_N' \end{bmatrix}'\end{aligned} \tag{2}$$

Note, not all initial conditions y_0 are measurable and/or physically meaningful — e.g. off-gas measurements. Thus the ARX model set may be expressed in matrix form

$$\bar{\boldsymbol{y}} - \boldsymbol{y} = -\boldsymbol{A}(\bar{\boldsymbol{y}}^0 - \boldsymbol{y}^0) + \boldsymbol{B}(\bar{\boldsymbol{u}} - \boldsymbol{u}) + \boldsymbol{w} \tag{3}$$

where $\boldsymbol{A}, \boldsymbol{B}$ are structured lower block triangular matrices. The profile $\boldsymbol{w}$ is a sequence of disturbance terms caused by bias in the reference input profile $\bar{\boldsymbol{u}}$, the effect of process upsets, and the modeling errors from linear approximations. This means that the disturbance $\boldsymbol{w}$ contains contributions from both batch wise persistent disturbances, such as recipe/input bias, model bias, and erroneous sensor readings, as well as from random disturbances, which occur with no batch wise correlation. It thus seems resoanble to model the disturbance profile $\boldsymbol{w}$ with a random walk model with respect to the batch index k

$$\boldsymbol{w}_k = \boldsymbol{w}_{k-1} + \boldsymbol{v}_k \tag{4}$$

where $\boldsymbol{v}_k$ represents a sequence of batch wise non-persistent disturbances that are assumed to be zero-mean, independent and identically distributed. The assumption of $\boldsymbol{v}_k$ being white is rather crude, but necessary if one whishes to keep the parameter estimation problem linear. Considering the difference between two successive batches

$$\Delta \boldsymbol{y}_k = \boldsymbol{y}_k - \boldsymbol{y}_{k-1} = \boldsymbol{A}\Delta \boldsymbol{y}_k^0 - \boldsymbol{B}\Delta \boldsymbol{u}_k + \boldsymbol{v}_k \quad (5)$$

A batch ARX model (5) that is independent of the reference profiles $(\bar{\boldsymbol{y}}, \bar{\boldsymbol{u}})$ and batch wise persistent disturbances has been obtained. With such a batch ARX model the path is prepared for multivariable, model-based monitoring, control, optimization, and of course simulation.

During the model derivation above it was assumed that the outputs are known. This is however not the case in practice, where only a sequence $\boldsymbol{z}_k$ of noisy observations of the outputs is available

$$\boldsymbol{z}_k = \left[\, y'_{k,0} \;\; \boldsymbol{y}'_k \, \right]' + \boldsymbol{\epsilon}_k \quad (6)$$

where $\boldsymbol{\epsilon}_k$ is a sequence of measurement noise terms that are assumed to be zero-mean, independent and identically distributed.

2.2 Application Specific Models

Depending on the task the batch ARX model (5) is to be applied to, it is convenient to convert the batch ARX model into different representations. If the task at hand is to predict (or simulate) the behavior of a batch before it is started the following form is convenient

$$\Delta \boldsymbol{y}_k = \boldsymbol{H}\Delta y_{k,0} - \boldsymbol{G}\Delta \boldsymbol{u}_k + \boldsymbol{E}\boldsymbol{v}_k \quad (7)$$

Note that the disturbance matrix $\boldsymbol{E}$ models the propagation of batch wise non-persistent disturbances — including batch wise non-persistent model-plant mismatch.

The form (7) above is also convenient for the task of classification/monitoring (e.g. normal or not) of a batch after it has been completed. Furthermore, the form (7) can be used to determine open-loop optimal recipes in the sense of optimizing an objective for the batch. If such an objective is to minimize the deviations $\boldsymbol{e}$ from a desired trajectory $\bar{\boldsymbol{y}}$, then (7) can be modified into

$$\boldsymbol{e}_k = \bar{\boldsymbol{y}} - \boldsymbol{y}_k = \boldsymbol{e}_{k-1} - \boldsymbol{H}\Delta y_{k,0} + \boldsymbol{G}\Delta \boldsymbol{u}_k - \boldsymbol{E}\boldsymbol{v}_k \quad (8)$$

There are two important points to be made about the trajectory tracking model form (8). First of all, as the error profile $\boldsymbol{e}_k$ in batch k depends on the error profile $\boldsymbol{e}_{k-1}$ from batch $k-1$, the effects of the batch wise persistent disturbances are integrated with respect to batch index. This means that a properly designed controller can reject the effects of the batch wise persistent disturbances asymptotically with respect to batch index — e.g. removing the effects of recipe and model bias. Secondly, given the above mentioned asymptotic behavior and as the control moves/actions generated by such a controller are deviations from the control/input profile realized in the previous batch, the control actions due to batch wise persistent disturbances will converge asymptotically to zero with respect to batch index. In literature it is said that the controller learns to reject the batch wise persistent disturbances — i.e. the resulting controller is an Iterative Learning Control (ILC) scheme. A more accurate formulation would be that both output and input errors are modeled using integrators with respect to batch index. The trajectory tracking model representation (8) is similar to that of Lee *et al.* (2000), but the representations differ significantly since (8) includes the effect of initial conditions ($\boldsymbol{H}\Delta y_{k,0}$) and disturbance propagation ($\boldsymbol{E}\boldsymbol{v}_k$). Another important difference is that (8) does not have double dependence on the batch wise persistent disturbances — i.e., the trajectory tracking model representation (8) only include the batch wise persistent disturbances as represented by $\boldsymbol{e}_{k-1}$ and not as both the part of $\boldsymbol{e}_{k-1}$ caused by the batch wise persistent disturbances and the batch wise persistent disturbances themselves.

The two forms (7) and (8) of the batch ARX model above are applicable to off-line or inter-batch type applications. For on-line estimation, monitoring, feedback control, and optimization however, it is convenient to use a state space realization of the batch ARX model. To achieve such a realization it is necessary to simplify the batch ARX model structure with the assumption that the number of outputs is constant $n_y(t) = n_y$ for $t = 1, \ldots, N$. In an observer canonical form the state space realization is given as

$$\begin{aligned} x_{k,t} &= \mathcal{A}_t x_{k,t-1} + \mathcal{B}_t \Delta u_{k,t-1} + \mathcal{E} v_{k,t} \\ \Delta y_{k,t} &= \mathcal{C} x_{k,t} \end{aligned} \quad (9)$$

with the initial condition $x_{k,0} = [\Delta y'_{k,0}, 0', \ldots, 0']'$. Just as (7), the SS model form (9) is convenient for prediction, monitoring, and optimization type applications, but also facilitates on-line implementations of these. Furthermore, the SS model form (9) is particularly well suited for closed-loop or feedback control applications. For tracking control applications the SS model form (9) can be modified into

$$\begin{aligned} x_{k,t} &= \mathcal{A}_t x_{k,t-1} + \mathcal{B}_t \Delta u_{k,t-1} + \mathcal{E} v_{k,t} \\ e_{k,t} &= e_{k-1,t} - \mathcal{C} x_{k,t} \end{aligned} \quad (10)$$

Following the discussion above, a multivariable feedback controller properly designed using the trajectory tracking SS model form (10), will reject the effects of the batch wise persistent disturbances asymptotically with respect to batch index. That is, due to the output and input error integration in the model framework, a controller designed to reject disturbances with respect to time in one batch at a time will also asymptotically reject the effects of batch wise persistent disturbances with respect to batch index.

3. MODEL IDENTIFICATION

With the batch ARX model (5) derived above, the parameterization of the batch model is in place, however the model orders and the model parameters still need to be determined from process data. One major drawback of the proposed parameterization is the immense dimensionality of the resulting set of models — in practice this immense dimensionality will render any standard Least Squares (LS) identification problem ill-conditioned. It turns out however, that as the grid-point models are progressively constrained by the smoothness of the model grid, the conditioning of the identification problem improves.

3.1 Data Pretreatment

In industry, the process variables $\tilde{z}_{k,\tilde{t}}(p) \in \mathbb{R}$ are most often logged individually at times $\tilde{T}(k,\tilde{t},p)$, giving $N_{\tilde{z}}(k,p)+1$ observations of variable p in batch k. What is needed however, is up to $N+1$ noise free observations of the variables at times $T(t)$ in the N_B batches available for identification. These noise free or expected observations can be estimated using local polynomial regression and If the profile of process variable p in batch k is defined as $\tilde{\boldsymbol{z}}_{k,p}$, then the estimation problem can be given explicitly (Hastie *et al.*, 2001) as

$$\hat{\tilde{z}}_{k,t}(p) = \boldsymbol{s}_{k,p,t}\tilde{\boldsymbol{z}}_{k,p} \tag{11}$$

where $\boldsymbol{s}_{k,p,t}$ is a smoothing vector. If it is further assumed that process variable p will be used throughout the batch, then the estimated profile of variable p in batch k is given as

$$\begin{aligned}\hat{\tilde{\boldsymbol{z}}}_k(p) &= \left[\begin{array}{cccc}\boldsymbol{s}'_{k,p,0} & \boldsymbol{s}'_{k,p,1} & \cdots & \boldsymbol{s}'_{k,p,N}\end{array}\right]' \tilde{\boldsymbol{z}}_k(p) \\ &= \boldsymbol{S}_{k,p}\tilde{\boldsymbol{z}}_k(p)\end{aligned} \tag{12}$$

Let the true observation $\bar{\boldsymbol{z}}_k \in \mathbb{R}^{(n_y(t)+n_u(t))}$ be given as

$$\bar{\boldsymbol{z}}_k = \hat{\bar{\boldsymbol{z}}}_k + \boldsymbol{\omega}_k \tag{13}$$

where $\hat{\bar{\boldsymbol{z}}}_k$ is the estimated observation and $\boldsymbol{\omega}_k$ is a sequence of estimation errors. The estimation error $\boldsymbol{\omega}_k$ will consist of both systematic errors such as the height of a characteristic peek being underestimated due to excessive smoothing and/or *trimming the hills and filling the valleys* due to too low local regression order, and random errors. Thus the estimation error $\boldsymbol{\omega}_k$ is modeled with a random walk with respect to the batch index k

$$\boldsymbol{\omega}_k = \boldsymbol{\omega}_{k-1} + \boldsymbol{\nu}_k \tag{14}$$

where $\boldsymbol{\nu}_k$ represents a sequence of batch wise non-persistent estimation errors that are assumed to be zero-mean. Consider the expected difference between two successive batches, then

$$E\{\Delta\bar{\boldsymbol{z}}_k\} = \hat{\bar{\boldsymbol{z}}}_k - \hat{\bar{\boldsymbol{z}}}_{k-1} + E\{\boldsymbol{\nu}_k\} = \Delta\hat{\bar{\boldsymbol{z}}}_k \tag{15}$$

is given as the difference between their respective estimates. The expected output and input difference profiles which are all contained in $\Delta\bar{\boldsymbol{z}}_k$, are thus given as

$$\begin{aligned}&E\{\Delta\boldsymbol{y}_k\} = \Delta\hat{\boldsymbol{y}}_k, \quad E\{\Delta\boldsymbol{y}^0_k\} = \Delta\hat{\boldsymbol{y}}^0_k \\ &E\{\Delta\boldsymbol{u}_k\} = \Delta\hat{\boldsymbol{u}}_k\end{aligned} \tag{16}$$

3.2 Parameter Estimation

Several suggestions to how (sets of) LTI or (periodic) LTV models should be identified from data can be found in literature. All these authors employ some or other coefficient shrinkage or subspace method to improve the conditioning of the identification problem and hence lower the variance of the model parameter estimates. Simoglou *et al.* (2002) suggested estimating a set of independent, overlapping local LTI SS models using Canonical Variant Analysis (CVA). Instead the present contribution proposes estimating a grid/set of interdependent grid-point LTI ARX models using a novel interpretation of generalized ridge regression.

The batch ARX model (5) can be formulated as linear regression

$$\Delta\boldsymbol{y}_k = \Delta\boldsymbol{x}_k\boldsymbol{\theta} + \boldsymbol{v}_k \tag{17}$$

where $\Delta\boldsymbol{x}_k = \Delta\boldsymbol{x}_k(\Delta\boldsymbol{y}^0_k, \Delta\boldsymbol{u}_k)$ is a structured regressor matrix with past outputs and inputs and $\boldsymbol{\theta} = \boldsymbol{\theta}(\boldsymbol{A},\boldsymbol{B})$ is a column parameter vector with the model parameters from the batch ARX model. Taking the expectation of the linear regression (17) and recalling (16) we find that

$$\Delta\hat{\boldsymbol{y}}_k = E\{\Delta\boldsymbol{x}_k\}\boldsymbol{\theta} + E\{\boldsymbol{v}_k\} = \Delta\hat{\boldsymbol{x}}_k\boldsymbol{\theta} \tag{18}$$

with $\Delta\hat{\boldsymbol{x}}_k = \Delta\boldsymbol{x}_k(\Delta\hat{\boldsymbol{y}}^0_k, \Delta\hat{\boldsymbol{u}}_k)$. This means that, if the process variable estimation error model (14) is a valid approximation, then estimation of model parameters from the pretreated data will give unbiased model parameter estimates. Although unbiased, model parameter estimates based on data from a single batch would have excessive variance. Thus to lower the variance of model parameter estimates, all available data should be used for the model parameter estimation

$$\begin{aligned}\boldsymbol{Y} &= \left[\begin{array}{cccc}\Delta\hat{\boldsymbol{y}}'_1 & \Delta\hat{\boldsymbol{y}}'_2 & \cdots & \Delta\hat{\boldsymbol{y}}'_{N_B}\end{array}\right]' \\ &= \left[\begin{array}{cccc}\Delta\hat{\boldsymbol{x}}'_1 & \Delta\hat{\boldsymbol{x}}'_2 & \cdots & \Delta\hat{\boldsymbol{x}}'_{N_B}\end{array}\right]'\boldsymbol{\theta} = \boldsymbol{X}\boldsymbol{\theta}\end{aligned} \tag{19}$$

The linear system (19) would however, most likely still be rank-deficient and solving it in a Least Squares (LS) sense would still produce estimates with low bias, but excessive variance. Such excessive model parameter variance would despite the low bias, yield poor model predictions (Larimore, 1996). Hence, to improve the predictive capabilities of an estimated model the variance of the estimated model parameters must be further reduced.

A possible approach to reducing the variance of model parameter estimates is to enforce that the estimated model possesses some desired model properties. One such model property could be that neighboring grid-point models are analogous in the sense that they exhibit similar behavior. In fact, without this property, the model would be a *set* of independent models and not a *grid* of interdependent models. Enforcing model properties however, inevitably introduce bias into the model parameter estimates. There will thus be a trade-off between the bias and variance of the model parameter estimates and this trade-off will determine the predictive capabilities of estimated models. A parameter estimation method that could incorporate model properties into LS estimates is generalized ridge regression, which also is referred to as Tikhonov regularization. We thus propose to estimate the model parameters by solving the extended LS problem

$$\begin{aligned}\hat{\boldsymbol{\theta}}(\boldsymbol{\Lambda}) &= \arg\min_{\boldsymbol{\theta}}[(\boldsymbol{Y}-\boldsymbol{X}\boldsymbol{\theta})'(\boldsymbol{Y}-\boldsymbol{X}\boldsymbol{\theta}) \\ &\qquad + (\boldsymbol{\Lambda}\boldsymbol{L}\boldsymbol{\theta})'(\boldsymbol{\Lambda}\boldsymbol{L}\boldsymbol{\theta})] \\ &= \left(\boldsymbol{X}'\boldsymbol{X}+\boldsymbol{L}'\boldsymbol{\Lambda}^2\boldsymbol{L}\right)^{-1}\boldsymbol{X}'\boldsymbol{Y}\end{aligned} \tag{20}$$

where the penalty $\boldsymbol{\Lambda}\boldsymbol{L}\boldsymbol{\theta}$ is a column vector of weighted differences between parameters in neighboring grid-point models. In this fashion, the structured penalty matrix $\boldsymbol{L}$ maps the parameter vector $\boldsymbol{\theta}$ into the desired parameter differences and the diagonal regularization matrix $\boldsymbol{\Lambda}$ weights the parameter differences. The estimated parameter vector $\hat{\boldsymbol{\theta}}(\boldsymbol{\Lambda})$ is a function of the regularization matrix $\boldsymbol{\Lambda}$, which determines the shrinkage and hence the trade-off between bias and variance. This means that the regularization matrix $\boldsymbol{\Lambda}$ can be used to tune the predictive capabilities of the model estimate. Through the particular choice of penalty matrix $\boldsymbol{L}$, the regularization matrix $\boldsymbol{\Lambda}$ also determines the interdependency between the grid-point models in the model grid.

3.3 Model Orders and Regularization Weights

Several methods for choosing (optimal) regularization weights can be found in literature (Hansen, 1996), but all of these consider either scalar regularization weights or diagonal penalties. In the present work it is proposed to simply select a regularization matrix from a finite set $\boldsymbol{\Lambda} \in \boldsymbol{\Omega}_{\boldsymbol{\Lambda}}$, that yield near minimum mean squared prediction error, when the estimated model is cross-validated through "pure-simulation". That is, given the "pure-simulation" prediction error profile $\boldsymbol{\zeta}_k(\boldsymbol{\Lambda})$ from cross-validation batch k

$$\boldsymbol{\zeta}_k(\boldsymbol{\Lambda}) = \Delta\hat{\boldsymbol{y}}_k^{val} - \hat{\boldsymbol{H}}(\boldsymbol{\Lambda})\Delta\hat{y}_{k,0}^{val} + \hat{\boldsymbol{G}}(\boldsymbol{\Lambda})\Delta\hat{\boldsymbol{u}}_k^{val} \tag{21}$$

the regularization matrix $\boldsymbol{\Lambda}$ is the solution to the discrete optimization problem

$$\begin{aligned}\boldsymbol{\Lambda} = \arg\min_{\boldsymbol{\Lambda}} &\left[\gamma(\boldsymbol{\Lambda}) = \sum_{k=1}^{N_B^{val}} \boldsymbol{\zeta}_k(\boldsymbol{\Lambda})'\boldsymbol{\zeta}_k(\boldsymbol{\Lambda})\right] \\ s.t.\quad &\boldsymbol{\Lambda} \in \boldsymbol{\Omega}_{\boldsymbol{\Lambda}} \\ &(\boldsymbol{X}'\boldsymbol{X}+\boldsymbol{L}'\boldsymbol{\Lambda}^2\boldsymbol{L}) \text{ nonsingular}\end{aligned} \tag{22}$$

where N_B^{val} is the number of batch difference profiles available for cross-validation. In this fashion, the computational burden of solving (22) is determined by the number of elements in the finite set $\boldsymbol{\Omega}_{\boldsymbol{\Lambda}}$.

Thus far only estimation of a specific batch ARX parameterization, i.e., a batch ARX model with model orders $n_A(t)$ and $n_B(t)$ for $t = 1, \ldots, N$ has been considered. These model orders are however unknown and will also have to be identified from data. This means that in addition to the regularization weighting matrix $\boldsymbol{\Lambda}$ also the model orders can be used to tune the predictive capabilities of the model estimate. Traditionally, ARX model orders are selected based on minimization of measures such as Final Prediction Error (FPE) or Akaike's Information Criterion (AIC) both of which are proportional to the optimal value of the LS objective being minimized as part of the identification, to prevent modeling noise/disturbance characteristics, i.e., overfit. Overfit is however also prevented if the ARX model orders are selected based on minimization of the mean squared prediction errors from cross-validation of the estimated models. This means that the ARX model orders can be selected based on minimization of

$$\begin{aligned}\begin{bmatrix}\{n_A(t)\}_{t=1}^N \\ \{n_B(t)\}_{t=1}^N\end{bmatrix} = \min_{\substack{\{n_A(t)\}_{t=1}^N \\ \{n_B(t)\}_{t=1}^N}} &[\gamma(\boldsymbol{\Lambda})] \\ s.t.\quad &\boldsymbol{\Lambda} \text{ given by (22)}\end{aligned} \tag{23}$$

If the ARX model orders are assumed constant throughout the batch $n_A = n_A(t)$ and $n_B = n_B(t)$ for $t = 1, \ldots, N$, then (23) simplifies to

$$\begin{aligned}(n_A, n_B) = \min_{n_A, n_B} &[\gamma(\boldsymbol{\Lambda})] \\ s.t.\quad &\boldsymbol{\Lambda} \text{ given by (22)}\end{aligned} \tag{24}$$

4. APPLICATION

To demonstrate the capability of the proposed data-driven models, an industrial, production scale *Bacillus protease* fermentation has been modeled from historical data (Novozymes A/S). The modeling objective was prediction of the on-line measured variables used to supervise the fermentation as well as the product activity which is measured sparsely off-line. That is, the objective was to obtain a model that can predict the course and outcome of a batch given the batch recipe and its initial conditions. For this *Bacillus protease* fermentation the batch recipe consists (essentially) of reference profiles for two

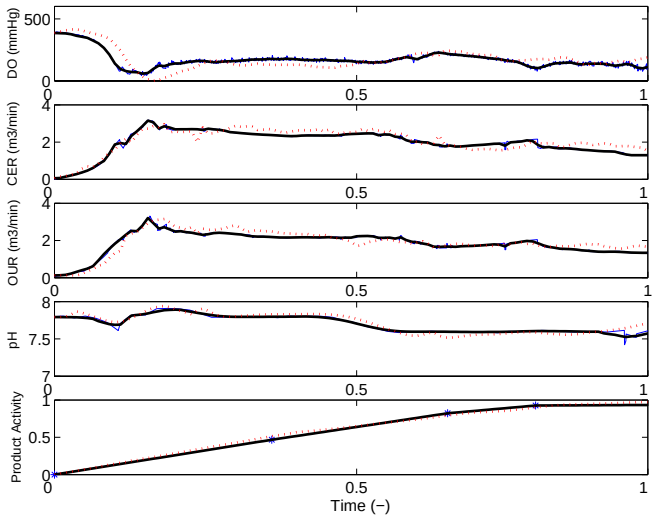

Fig. 1. Example of cross-validation of an industrial *Bacillus protease* fermentation model. The five outputs, Dissolved Oxygen (DO), Carbon dioxide Evolution Rate (CER), Oxygen Uptake Rate (OUR), pH, and product activity, are predicted given information about their initial conditions and the batch recipe (assuming perfect control) — i.e., *pure-simulation* prediction. The thin solid lines (or '$*$' for the product activity) are the historical measurements as logged, the bold solid lines are the pretreated data (as the data from which the model was identified, but not used in the identification), and the dotted lines are the model predictions.

substrate feeds, an alkaline feed, pressure, and temperature — i.e., these reference profiles are the inputs of the model. For most of these inputs the current practice is however, that the reference profile is either not logged or not manipulated from batch to batch. As a temporary workaround, perfect control was assumed and the reference profiles were replaced by the realized profiles. As is common practice in supervision of fermenters, Dissolved Oxygen (DO), Carbon dioxide Evolution Rate (CER), Oxygen Uptake Rate (OUR), and pH were chosen as process indicators. Along with the product activity these process indicators makeup the outputs of the model.

The historical data was smoothened and re-sampled to 30 minutes intervals. The product activity was re-sampled using linear interpolation, while the remaining inputs and outputs were smoothened using local constant regression and bandwidths ranging from 6 to 73 nearest neighbors. Before identification the batch difference profiles were normalized. The model was identified using data from 29 batches and cross-validated using data from 9 batches, one of which is shown in figure 1. The identified model orders ranged from 0 to 20 and the total number of model parameters estimated was 12,135. The mean cross-validation prediction error was 0.13.

5. CONCLUSION

In the present paper it is proposed to model finite horizon, time-varying and nonlinear process operations with 1-dimensional grids of interdependent ARX models. Such model grids can be used for both off- and on-line monitoring, prediction, control, and optimization applications. It is further proposed that these model grids are identified from historical process data using ridge regression. By identifying all the ARX models in a model grid simultaneously, the interdependency of the ARX models can be used to reduce the variance of their estimates and thereby improve the predictive capabilities of the estimated model grid. The proposed data-driven modeling scheme has been demonstrated through modeling of an industrial fermentation process.

REFERENCES

Hansen, Per Christian (1996). *Rank-Deficient and Discrete Ill-Posed Problems*. Polyteknisk Forlag. Lyngby.

Hastie, Travor, Robert Tibshirani and Jerome Friedman (2001). *The Elements of Statistical Learning*. Springer. New York.

Larimore, Wallace E. (1996). Statistical optimality and canonical variate analysis system identification. *Signal Processing* **52**(2), 131–144.

Lee, Jay H., Kwang S. Lee and Won C. Kim (2000). Model-based iterative learning control with a quadratic criterion for time-varying linear systems. *Automatica* **36**(5), 641–657.

Simoglou, A., E. B. Martin and A. J. Morris (2002). Statistical performance monitoring of dynamic multivariate processes using state space modelling. *Computers and Chemical Engineering* **26**(6), 909 – 920.

TWO-DIMENSIONAL POPULATION BALANCE MODELLING OF SEMI-BATCH ORGANIC SOLUTION CRYSTALLIZATION

Puel, F. and Févotte, G.

LAGEP, UMR CNRS 5007, Université Lyon 1, 43 bld. Du 11 novembre 1918. 69100 Villeurbanne. FRANCE

Abstract: A population balance model simulates the time variations of two characteristic sizes of hydroquinone particles during crystallization. The population balance equations combined with kinetic models and mass balance equations allowed the simulation of the crystallization of hydroquinone characterized by a rod-like habit. Semi continuous isothermal operations were performed at the lab-scale in the presence of various additive concentrations. Both the experimental supersaturation trajectory and the final bi-dimensional Crystals Size Distribution (CSD) were correctly predicted by the model. The simulated elongation factor characterizing the crystal shape was therefore in agreement with the experimental one. For secondary nucleation, indirect effects were assumed to occur and satisfactory predictions of the final number of fine particles were obtained. A major interest of the two-dimensional model lies in its ability to relate the time variations of the crystal habit : the particles lengthen in the first moments of their growth and then progressively get thicker until the end of the process.

Keywords: Modelling, Particulate Processing, Parameter Estimation, Chemical Industry, Partial Differential Equations, Batch Processes.

1. INTRODUCTION

In the field of industrial crystallization most authors have focused their efforts on modelling one characteristic parameter of the particles, generally a given equivalent size (Franck et al., 1988; David et al., 1991). Nevertheless, the usual one-dimensional approach does not suitably describe the evolution of a population of anisotropic crystals, which is the common case with organic products. This is why a two dimensional population balance approach was presented and solved numerically (Puel et al., 2003a), in order to simulate the time variations of two sizes of crystals. Actually, the industrial production of fine organics may lead to problems arising from the lack of mastery of the end-use properties of the crystals. These problems are due to the high sensitivity of the crystal habits to the effects of supersaturation, impurities and additives during the crystallization operation. It is therefore useful to analyse and predict the evolution of crystal habits during the process.

At the solid state, hydroquinone exhibits a rod like habit (see Fig.1), with three main dimensions: length L_1, width L_2 and height, assumed to be equal to the width. An elongation shape factor, F_1, is also defined as the length to width ratio. To take into account the two sizes and the shape of the crystals, two-dimensional population balance equations are required. Such modelling strategy will be applied to determine the kinetic parameters of the crystallization process.

Batch experiments have rich information contents and are therefore suitable for satisfactory parameter estimation of the nucleation and growth mechanisms. However the time variations of temperature require taking into account the temperature dependency of the kinetic parameters. Consequently, isothermal semi-batch operation appears as a good strategy to obtain a set of kinetic parameters since it allows distinguishing between the various phenomena occurring as a function of time. At the beginning, the process is dominated by primary nucleation, afterwards the crystal growth gets the upper hand,

and secondary nucleation takes a significant part in the size variations when the concentration of crystals is sufficient. The crystallization of hydroquinone was therefore experi-mentally carried out in a semi-batch isothermal well-mixed crystallizer. In addition to usual kinetic investigations, the effect of various concentrations of a tailor-made additive was also studied. The semi-batch crystallization of hydroquinone was then simulated using a bi-dimensional population balance approach.

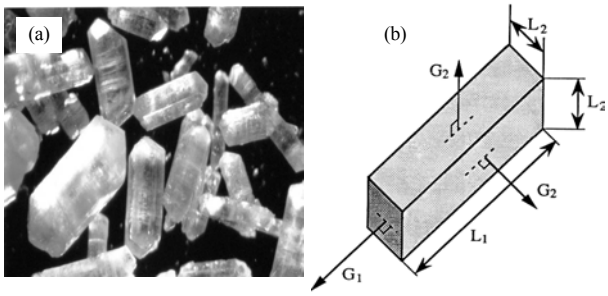

Fig. 1. (a) Photographic picture of typical crystals of hydroquinone and (b) bi-dimensional approxi-mation of the corresponding rod-like particles.

2. EXPERIMENTAL SETUP AND OPERATING CONDITIONS

2.1 Experimental setup

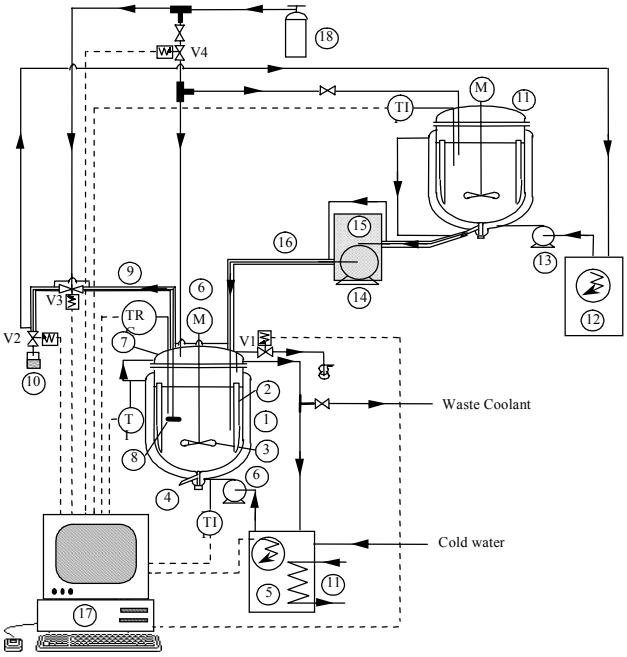

Fig. 2. Experimental apparatus

The experimental device is shown schematically in Fig. 2. The crystallizer (1) is a glass reactor equipped with four baffles (2) and a Mixell TT propeller (3). The suspension is withdrawn from the vessel using the bottom valve (4). A constant temperature is maintained in the crystallizer by using a thermostatic bath (5) and a circulating pump (6). The coolant goes through a glass jacket and a jacketed cover (7). Four electrovalves were sequentially manipulated to perform the withdrawal of solution samples through a filter (8). Samples were diluted for titration. The feed tank (11) was thermostated (12), the transfer of the hot undersaturated solution to the crystallizer was carried out using a peristaltic pump (14) and jacketed pipes (16). The required temperature measurements were obtained using Pt100 probes. Nitrogen (18) was fed in the two vessels to prevent oxidation in solution.

2.2 Fed-batch isothermal crystallization experiments

The crystallizer was initially filled with a saturated solution of hydroquinone, and kept at 25°C. During the first period of the semi-continuous operation (i.e. the first half an hour) a 'hot' solution was fed to the crystallizer. Afterwards, the suspension was kept at 25°C, under stirring, for about 1.5 hour, in order to let the slurry reach the equilibrium. Samples of the clear liquor in the crystallizer were withdrawn every 3 minutes. The solute concentration of these samples was determined through titration. The two dimensional crystal size distributions of final crystal samples were measured using image analysis.

3. EXPERIMENTAL RESULTS

3.1 Supersaturation profiles

The solute concentration data allowed the computation of the degree of supersaturation β, defined as the ratio of the solute concentration to the solubility.
A semi batch run (see Fig.3) consists of three phases. During phase 1, the solute concentration increases as the feeding solution presents a higher hydroquinone concentration. Phase 1 terminates when primary nucleation occurs. During phase 2 the solute concentration reaches a plateau: the feeding rate of hydroquinone is then constant and equal to the rate of consumption through particles growth. Phase 3 begins when the feeding rate falls to zero. A decrease of the solute concentration towards the solubility is then observed.
As expected, the presented experimental data also show that supersaturation tends to 0 at the end of phase 3.

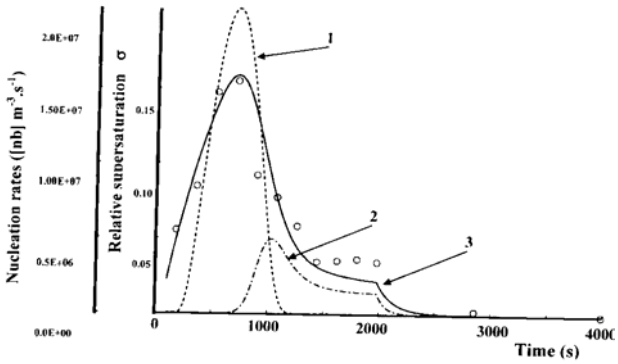

Fig. 3. Semi batch crystallization of hydroquinone Computed nucleation rates (dashed lines 1 and 2 for r_{N1} and r_{N2}); computed relative supersaturation σ (full line 3); measurements of the relative supersaturation σ (open circles)

3.2 Evolution of crystals sizes and elongation factor

To avoid undesirable thin needle crystal habits, a tailor-made additive was selected for its ability to reduce the growth along the length direction. The efficiency of such addition was clearly demonstrated

as the average length decreased with the additive concentration. The measured coefficients of variation are rather large: a unique period of crystals birth (i.e. through primary nucleation) is not consistent with such wide CSD. Consequently, secondary nucleation phenomena have to be considered for realistic further simulations.

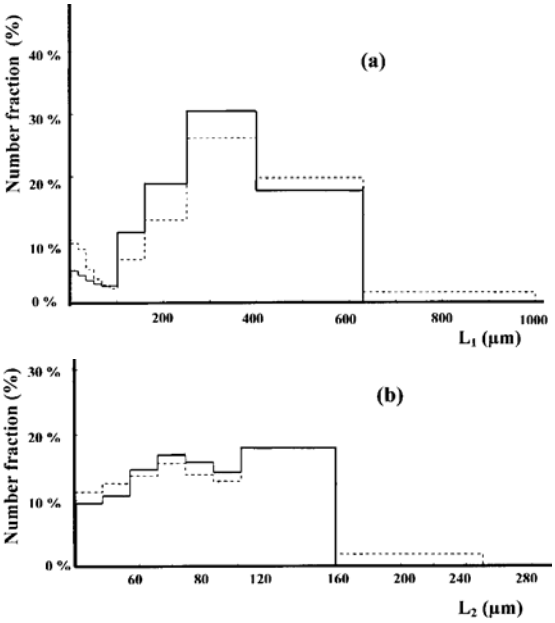

Fig. 4. Semi batch crystallization of hydroquinone (run SC2): Comparison between computed and measured number CSD of final crystals (a) Length L_1; (b) Width L_2. (Dashed lines: Measurements using Image Analysis; Full lines: Computed Final CSD)

Indeed, the size- and impurity-dependency of F_1 cannot be expressed by any simple and obvious relationship. For example, no satisfactory simulation of the variations of the crystal shape can be obtained assuming a constant elongation factor over the size range. Therefore, considering two dimensional population balances in the case of non-isotropic crystals presents a real interest for predictive modelling purposes. Obviously, the experimental data required for such modelling cannot be obtained through usual particle sizing techniques such as laser diffraction methods, as they only provide one equivalent size distribution. This is why image analysis was used (Fig.4)

4. ESTIMATION OF THE KINETIC PARAMETERS OF THE CRYSTALLIZATION

4.1 Kinetic modelling of the semi batch crystallization of hydroquinone

The main mechanisms encountered in the semi-batch crystallization of hydroquinone are primary and secondary nucleation, and growth. In the modelling breakage and agglomeration were assumed to be of second order of importance.

A detailed model describing the crystallization of hydroquinone, based on bi-dimensional population balance equations (PBE), was developed to compute the time variations of L_1 and L_2. The CSD was assumed not to depend on spatial coordinates in the well-mixed lab-scale crystallizer. The PBEs involve kinetics equations relating the mechanisms of crystallization mentioned above and mass balance equations. The whole model is presented in more details by Puel et al. (2003a). Table 1 summarizes the main equations which were considered in the case of well-mixed crystallizers.

A, B are primary nucleation coefficients that can be determined experimentally and have complex physical meaning (see e.g. Mersmann, 1996). k_N, *n, k* are parameters for the kinetic modelling of secondary nucleation. k_N is generally assumed to be related to the stirring power and to exhibit a temperature-dependency according to Arrhenius's law. Exponent *n* lies between 0.5 and 2.5. Exponent *k* is generally assumed to be of the order of 1 (Garside, 1985). $k_{i,1}$, $k_{i,2}$, j_1 and j_2 are growth parameters for the integration step of solute in the crystal lattice. $k_{i,1}$ and $k_{i,2}$ are the kinetic constants related to L_1 and L_2 directions, respectively, and j_1 and j_2 (in general 1 or 2) are the order of integration depending on the mechanism in question. k_d, is a mass transfer coefficient related to the diffusive step of solute in the layer around the crystal surface. η_1 and η_2 are effectiveness factors for faces 1 and 2 allowing to calculate the real mass flux density integrated in the crystal with respect to the maximal mass flux density that would be obtained in the absence of diffusive limitations (Garside, 1971).

Twelve parameters are thus involved, but the last three ones, which are time varying, can be calculated for every time step, using data available in the literature. Finally, nine kinetic parameters remain to be estimated from the experimental data through the fitting of the measured variables to the model-predicted ones.

4.2 Solving the bi-dimensional Population Balance Equations (PBE)

The method of classes was used for solving the bi-dimensional PBE, it requires the introduction of population number function $N(L_1,L_2,t)$. The crystals number function is discretized over the bi-dimensional size domain and $Ni,j(t)$ represents the number of crystals belonging to the class denoted by $Cl_{i,j}$. The program calculates the relative supersaturation σ, the kinetic rates of nucleation r_{N1} and r_{N2} and of growth G_1 and G_2 along the L_1 direction, respectively the L_2, axes. The total number and mass of crystals and the bi-dimensional size distribution are finally computed.

The spatial domain of crystals length and width (respectively L_1 and L_2) is first discretized and the smallest class of size is assumed to fit the characteristic nuclei represented by its two dimensions, L_1^* and L_2^*.

Let $L_{1,0}$,..$L_{1,i}$, ...$L_{1,im}$ be a suite of length where $L_{1,im}$ is the length of the largest crystals. These lengths define *im* classes quoted $Cl_{1,i}$, the extent of a class is $\Delta Cl_{1,i} = L_{1,i} - L_{1,i-1}$ and the characteristic length of the class is $S_{1,i} = (L_{1,i-1} + L_{1,i})/2$. The same discretization is performed for L_2.

As Fig.5 shows, such discretization defines bidimensional classes $Cl_{i,j}$, delimited by $L_{1,i}$, $L_{1,i-1}$, and $L_{2,j}$, $L_{2,j-1}$ of area $A_{i,j} = \Delta Cl_{1,i}\ \Delta Cl_{2,j}$. These classes are fixed and of constant size. The size domain is divided

in a system of *im* by *jm* bi-dimensional classes. The method of classes also requires the introduction of the population number function $N(L_1,L_2,t)$ defined as follows :

$$\frac{d^2N(L_1,L_2,t)}{dL_1 dL_2} = \psi(L_1,L_2,t) \quad (1)$$

The number of crystals belonging to the class $Cl_{i,j}$ can therefore be expressed as :

$$N_{i,j}(t) = \int_{L_{i-1}}^{L_i}\int_{L_{j-1}}^{L_j} \psi(L_1,L_2,t)dL_1dL_2 \quad (2)$$

im by *jm* number functions $N_{i,j}(t)$ are thus defined.

4.3 Application of the method of classes

To express the population balance equations, the population number function $N(L_1,L_2,t)$ are now used, rather than the population density function $\psi(L_1,L_2,t)$.

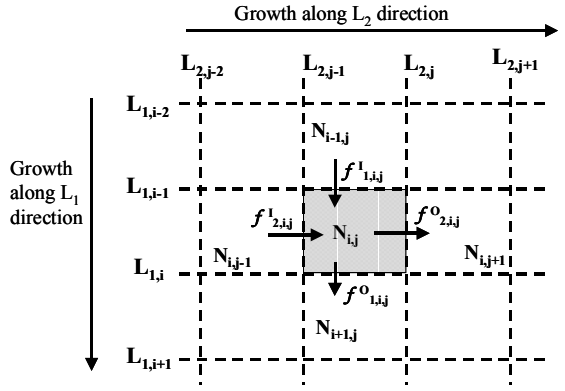

Fig. 5. Bi-dimensional class $Cl_{i,j}$, inlet flows of crystal numbers $f^{I}_{1,i,j}$; $f^{I}_{2,i,j}$ and outlet flows of crystal numbers $f^{O}_{1,i,j}$; $f^{O}_{2,i,j,}(t)$

1. The balance equation (T1) (see Table 1) is first discretized according to the bi-dimensional grid presented above (see also Fig.5):
The PBE is integrated after combining expressions (2) and (T1) with :

$$\int_0^\infty\int_0^\infty R_N dL_1 dL_2 = r_{N1} + r_{N2} \quad (3)$$

2. The population balance around the bi-dimensional class $Cl_{i,j}$ leads to a set of *im* by *jm* ordinary differential equations :

$$\frac{1}{V_T(t)}\frac{d}{dt}\left[N_{i,j}(t)V_T(t)\right] + f_{1,i,j}(t) + f_{2,i,j}(t) + \quad (4)$$

$$+\frac{F(t)N(L_1,L_2,t) - F_{in}(t)N_{in}(L_1,L_2,t)}{V_T(t)} = r_{N1} + r_{N2}$$

$f_{1,i,j}(t)$ and $f_{2,i,j}(t)$ are the net inlet and outlet flows of crystals in class $Cl_{i,j}$, in the length and width directions induced by growth, respectively. Each crystals flow being divided in inlet and outlet flows for each direction (see arrows on Fig.5)

$$f_{1,i,j,}(t) = f^{O}_{1,i,j,}(t) - f^{I}_{1,i,j,}(t) \quad \text{and}$$
$$f_{2,i,j,}(t) = f^{O}_{2,i,j,}(t) - f^{I}_{2,i,j,}(t) \quad (5)$$

Where $f^{O}_{1,i,j}(t)$, $f^{O}_{2,i,j}(t)$ are the outlet crystal flows from the $Cl_{i,j}$ class in the L_1 and L_2 directions ; and $f^{I}_{1,i,j}(t)$, $f^{I}_{2,i,j}(t)$ are the inlet crystal flows from the $Cl_{i,j}$ class in the L_1 and L_2 directions

The calculation of these inlet and outlet crystal fluxes are carried out using a first-order Tailor series expansion:

$$f^{O}_{1,i,j}(t) = G_1(S_{1,i},t)\left[a_{1,i}N_{i,j}(t) + b_{1,i}N_{i+1,j}(t)\right] \quad (6)$$

$$f^{I}_{1,i,j}(t) = G_1(S_{1,i-1},t)\left[a_{1,i-1}N_{i-1,j}(t) + b_{1,i-1}N_{i,j}(t)\right]$$

with $$a_{1,i} = \frac{\Delta Cl_{1,i+1}}{\Delta Cl_{1,i}(\Delta Cl_{1,i+1} + \Delta Cl_{1,i})} \quad (7)$$

$$b_{1,i} = \frac{\Delta Cl_{1,i}}{\Delta Cl_{1,i+1}(\Delta Cl_{1,i+1} + \Delta Cl_{1,i})} \quad (19)$$

and $$f^{O}_{2,i,j}(t) = G_2(S_{2,j},t)\left[a_{2,j}N_{i,j}(t) + b_{2,j}N_{i,j+1}(t)\right] \quad (8)$$

$$f^{I}_{2,i,j}(t) = G_2(S_{2,j-1},t)\left[c_{j-1}N_{i,j-1}(t) + d_{j-1}N_{i,j}(t)\right]$$

with $$a_{2,j} = \frac{\Delta Cl_{2,j+1}}{\Delta Cl_{2,j}(\Delta Cl_{2,j+1} + \Delta Cl_{2,j})} \quad (9)$$

$$b_{2,j} = \frac{\Delta Cl_{2,j}}{\Delta Cl_{2,j+1}(\Delta Cl_{2,j+1} + \Delta Cl_{2,j})}$$

The previous expressions are valid for $2<i<im-1$ and $2<j<jm-1$. Only four neighbouring classes of $Cl_{i,j}$ are considered in the design of the algorithm. Particular cases are considered for the classes which are set at the boundaries of the size domain. The lower classes can not accept growing crystals form the previous ones: $f^{I}_{1,1,j}(t) = f^{I}_{2,i,1}(t) = 0$. Crystals in the upper classes can not grow in the next ones: $f^{O}_{1,im,j}(t) = f^{O}_{2,i,jm}(t) = 0$. Other numerical treatments are necessary and are reported by Puel (1994).

4.4 Parameter estimation and simulation results

Data were collected after six experiments which correspond to four concentrations of tailor-made additive (i.e. 0, 400, 600 and 1000 ppm).
'Usual' optimisation procedures would obviously lead to an excessive computational time and are likely to converge towards local optima. The applied estimation strategy was therefore based on the use of mechanistic knowledge of the crystallization system to save time and to make the convergence easier. Such strategy was successfully applied by David et al. (1991), it is based on the fact that different mechanisms occur successively during this semi batch crystallization process: as outlined above there are 3 main periods during which each mechanism prevails even though until the end of the process, secondary nucleation should be considered as a potential mechanism for the generation of nuclei. In practice the estimation procedure is therefore driven as follows:
Firstly, the exponents involved in the growth kinetic are arbitrarily fixed at $j_1=j_2=1$. The CSD is computed and the calculated and measured mono-dimensional crystals distributions are compared, successively in the L_1 and L_2 directions. To stress on the bi-dimensional information, the simulated and experimental elongation factor F_1 are also compared. By this way, a precise choice of the kinetic orders n, k , j_1 and j_2 can be performed. The values of A, B, k_N, $k_{i,1}$ and $k_{i,2}$ are then tuned using a trial and error approach based on the physical meaning of the parameters which have to be estimated. More details

on the parameter estimation are reported by Puel et al. (2003b).

Run SC4. Run SC4, carried out with 600 ppm of additive, was first selected. Fig. 3 presents the measured and calculated relative supersaturation. The model prediction is good until the supersaturation reaches the plateau, where the simulation underestimates the steady-state supersaturation. The obtained value of B is rather low, leading to a large burst of primary nucleation peak during few minutes. Actually, A and B are strongly linked together through the total number of crystals, a reduction of B leads to an increase of A. Nevertheless, the maximum estimated supersaturation value, which corresponds to the limit of the metastable zone, is correctly predicted. The kinetic coefficients and orders of secondary nucleation were then fitted to represent the population of fine crystals in the final CSD (see Fig. 4)). Again, the four kinetic parameters related to the two growth laws are strongly connected. Values 1 and 2 for the orders j_1 and j_2 lead to 4 possible combinations. Setting $j_1=j_2=2$ or $j_1=j_2=1$ leads to underestimate, respectively overestimate, the decrease of supersaturation after primary nucleation. Additional information was then obtained from the measurements of the elongation factor F_1, which is very sensitive to differences in the growth rates along the two main directions. Finally, setting $j_1=2$ and $j_2=1$ allowed the best prediction of the particle shape. Any other value of j_1 and j_2 leading to a maximum for F_1, which was not experimentally observed. The growth coefficients $k_{i,1}$ and $k_{i,2}$ were finally set considering the main population of crystals in the final distribution (see Fig. 4). For the experiment in question, the length and width of crystals were satisfactorily predicted.

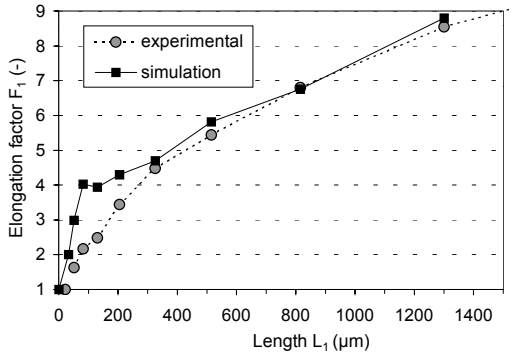

Fig. 6. Semi-batch crystallization of hydroquinone (run SC1). Experimental and model-predicted evolution of the elongation shape factor F_1 vs. L_1 (Average of a sample of final crystals)

Runs SC1, SC2 and SC5. Some of the kinetic parameters estimated after run SC4 should be modified in order to account for the effect of the concentration of additive.

The orders of the growth and secondary nucleation kinetic laws (n, k, j_1 , j_2) were unchanged since no modification of the two mechanisms involved was expected from the introduction of additive. Due to the chemical structure of the additive, it was also assumed that the growth in the L_2 direction was not altered so that $k_{i,2}$ was kept constant. Moreover the experiments showed that primary nucleation was increasingly delayed by increasing amounts of additive. Parameters A and B being linked each other, A was assumed constant and then B fitted in order to represent the measured maximal supersaturation in the neighbourhood of primary nucleation. The level of fine particles in the CSD and the final total number of crystals is dependent on the primary and secondary nucleations. The prediction of the number of crystals was achieved through the evaluation of appropriate values of the kinetic coefficients B and k_N related to the law for nucleations. Moreover, in order to reproduce the reduction of the experimental elongation factor with increasing concentrations of additive – which, indeed, is the effect expected from the use of the selected additive – it was necessary to assess a decreasing relationship between the value of $k_{i,1}$ and the concentration of additive.

The three parameters mentioned above (i.e. B, k_N and $k_{i,1}$) were first estimated for runs SC2 (400 ppm of additive) and SC5 (1000 ppm of additive) by comparing experimental and simulation results. The fit obtained between experimental and simulated data was correct. Unfortunately, for run SC1 (0 ppm of additive), no supersaturation measurement was available. Consequently, in order to extend the set of kinetic parameter values, the missing parameters of B, k_N *and* $k_{i,1}$ were extrapolated at 0 ppm. Second order polynomial and linear relationships between the three kinetic parameters and the concentration of additives were established As one can see in Fig. 6, the simulated elongation factor for run SC1 obtained with the extrapolated parameters at 0 ppm was in good agreement with the experimental data, the model and the set of kinetics parameters were therefore considered as validated.

5. GENERAL REMARKS AND DISCUSSION OF THE RESULTS

As far as the estimation of numerous kinetic parameters is involved, it is our opinion that, given the limited number of experimental data and the complexity of the crystallization phenomena, the use of an optimization algorithm would lead to uncertain parameters and finally to a poor predictive ability of the model. Putting physical knowledge in the modeling allowed more efficient and more reliable convergence towards a satisfactory representation of the semi-batch crystallization operations.

The main originality of the present work lies in its two-dimensional approach for the modeling of particle shape, and almost no such application based on real experimental data can be found in the literature. This work is also an attempt to relate the effect of a specific tailor-made additive to the shape of hydroquinone crystal.

Primary nucleation appears to be quite sensitive to the concentration of additive as the delay of nuclei formation increases with the additive concentration. The molecules of additive turn out to act as nucleation inhibitors, maybe by limiting the growth of crystal embryos. The concentration dependency of parameter B estimated during the present work relates the increase of the width of metastable zone associated to such inhibition effect. Secondary

nucleation was taken into account to explain the fractions of fine crystals in the final experimental CSD, even though this is not the major mechanism for nuclei generation.

A major impact of the additive on the crystal habit was also observed and simulated. The molecules of additive act as efficient growth inhibitors in the length direction so that between 0 and 1000 ppm, the growth rate kinetic coefficient $k_{i,1}$ is divided by a factor of 3.2. Again, this result is consistent with physical considerations.

6. CONCLUSIONS

A bi-dimensional population balance approach was developed for simulating the time variations of the habit of non isotropic crystals of hydroquinone during solution crystallizations. The algorithm coupled with kinetic models allowed the simulation of isothermal semi-batch crystallization of hydroquinone exhibiting a rod-like habit. Despite various experimental conditions, the supersaturation profiles were correctly predicted, and the computed final bi-dimensional CSD and elongation shape factors fit the experimental data.

An inhibition effect of a tailor made additive was clearly observed, and represented by the model. The additive mainly affects primary nucleation and the growth in the length direction, but secondary nucleation mechanisms and their inhibition in the presence of additive were also taken into account and successfully represented, allowing a good prediction of the final content of the slurry in fines particles.

A set of nine kinetics parameters was estimated through the comparison between experimental and calculated data.

The reported parameter values were partly validated trough the prediction of a semi-batch crystallization performed without additive. Three kinetic parameters were related to the concentration of additive in order to represent the inhibition effects of the tailor-made additive but, even though their physical consistency was justified, the obtained relationships are simply phenomenological.

REFERENCES

David R., J., Villermaux, P., Marchal, J.P. Klein (1991).Crystallization and precipitation engineering – IV. Kinetic model of adipic acid crystallization. *Chem. Eng. Sci.*, **46**,4,1129-1136.

Franck R., R., David, J., Villermaux, J.P., Klein (1988). Crystallization and precipitation engineering. II. A chemical reaction engineering approach to salicylic acid precipitation. *Chem. Eng. Sci.*, **43**,1,69-77

Garside, J. (1971). The concept of effectiveness factors in crystal growth. *Chem. Eng. Sci.*, **26**, 1425-1431.

Garside, J. (1985). Industrial crystallization from solution. *Chem. Eng. Sci.*, **40**,1,3-26.

Mersmann, A., (1996). Supersaturation and nucleation. *Trans.IChem E.,* **74**, Part A, 812-820.

Puel, F. (1994). Bilan de population pour deux tailles caractéristiques de particules : application à la crystallisation de l'hydroquinone. Ph-D Thesis Université Lyon 1, (in French)

Puel F., G., Fevotte, J.P., Klein. (2003a). Simulation and analysis of industrial crystallization processes through multidimensional population balance equations. Part 1: A resolution algorithm based on the method of classes. To appear in *Chem. Eng. Sci*

Puel F., G., Fevotte, J.P., Klein. (2003b). Simulation and analysis of industrial crystallization processes through multidimensional population balance equations. Part 2: A study of semi batch crystallization. To appear in *Chem. Eng. Sci.*,

Table 1. Main equations of the crystallization model in the case of well-mixed crystallizers

Population balance for two main sizes (L_1 and L_2)	$\frac{1}{V_T(t)}\frac{\partial}{\partial t}\left[\psi(L_1,L_2,t)V_T(t)\right]+\frac{\partial}{\partial L_1}\left[G_1(L_1,t)\psi(L_1,L_2,t)\right]+\frac{\partial}{\partial L_2}\left[G_2(L_2,t)\psi(L_1,L_2,t)\right]$ $+\frac{F(t)\psi(L_1,L_2,t)-F_{in}(t)\psi_{in}(L_1,L_2,t)}{V_T(t)}=R_N(L_1,L_2,t)$	(T1)
	with $\int_0^{\infty}\int_0^{\infty} R_N\,dL_1dL_2=\int_0^{L_1^*}\int_0^{L_2^*} R_N\,dL_1dL_2=r_{N1}+r_{N2}$	(T2)
Primary nucleation	$r_{N1}=A.\exp\left(-\frac{B}{\ln^2\beta}\right)$	(T3)
Secondary nucleation	$r_{N2}=k_N.\sigma^n M_T^k$	(T4)
Growth L_1 direction	$G_1(t)=2\frac{M_s}{\rho_s}\eta_1.k_{i,1}(C(t)-C^*(T(t))^{j_1}$ with	(T5)
	$\left[\frac{k_{i,1}}{k_d}[C(t)-C^*(T(t))]^{j_1-1}\right]\eta_1+\eta_1^{1/j_1}-1=0$	
Growth L_2 direction	$G_2(t)=2\frac{M_s}{\rho_s}\eta_2.k_{i,2}(C(t)-C^*(T(t))^{j_2}$ with	(T6)
	$\left[\frac{k_{i,2}}{k_d}[C(t)-C^*(T(t))]^{j_2-1}\right]\eta_2+\eta_2^{1/j_2}-1=0$	
Mass balance	$f_{in}(t)C_{in}(t)=F_{in}(t)C_{in}(t)=\frac{d\left[V(t)C(t)+V_T(t)C_s(t)\right]}{dt}$	(T7)

CALORIMETRIC ESTIMATION OF VISCOSITY AND ACID NUMBER IN ALKYD REACTORS

Isabel Sáenz de Buruaga[1], Teresa López[2], Sandra Pérez[2], and Jesús Alvarez[2]

[1] Centro de Investigación en Polímeros (CIP)
Marcos Achar Lobatón # 2, 55855 Tepexpan Edo. de México, MÉXICO
[2] Universidad Autónoma Metropolitana-Iztapalapa
Depto. de Ingeniería de Procesos e Hidráulica
Apdo. 55534, 09340 México D.F, MÉXICO

Abstract: In the industrial operation of batch alkyd polymerization reactors, the process evolution is monitored by measuring the acidity and the viscosity of samples withdrawn from the reactor. The synthesis is stopped at the maximum yield allowed by the gelation point of the cold product. In this work, a software sensor that estimates the C(cold)-viscosity and the conversion of acid groups on the basis of the continuous measurement of the heat exchange rate between a continuous stirred vessel appended to the reactor and a cooling coil is designed and experimentally tested. The identification of the underlying time-varying observability property yields the designs of the heat exchange devise and of the corresponding robust nonlinear geometric observer. The resulting software sensor is experimentally tested in a pilot plant reactor.

Keywords: polymer reactor, cold-viscosity, acid number, alkyd reactor, calorimetric estimator, nonlinear observer, software sensor.

1. INTRODUCTION

Oil-modified polyesters, commonly known as alkyd resins, have a high demand as coating resins due to their low production cost and variety of properties (durability, color retention, brightness, etc.). Commonly, an industrial batch alkyd cook is monitored, controlled and stopped on the basis of discrete-delayed measurements of acidity and C(cold)-viscosity. The acidity measures the conversion of monomers into polymer, and the C-viscosity reflects the complex branched molecular architecture of the polymer. The batch must be stopped at a certain conversion below the gelation point of the cold product. A drift from the prescribed C-viscosity trajectory signifies that the polymer structure is drifting from its nominal value, and an abrupt change means that the cook is running away from its nominal motion. Recently, on-line continuous measurements of C-viscosity have been considered (Händel, 1996) to improve the monitoring and control schemes via a continuous sampling-cooling loop with a viscosimeter. However, this scheme has the drawback of the investment and maintenance costs associated to the *in situ* operation of a viscosimeter instrument.

Due to the lack of reliable kinetic models and the uncertainty of the monomers structure (Patton, 1962), the standard nonlinear extended Kalman filter and Luenberguer model-based observer techniques (Eliçabe and Meira, 1988; Mutha *et al*., 1997; Alvarez and López, 1999, Ellis *et al*. 1994) cannot be directly applied to alkyd reactors. To overcome this problem, López *et al*. (2000) designed a geometric estimator on the basis of an uncertain kinetic model augmented with an observable (i.e., adjustable) parameter and discrete-delayed measurements of C-viscosity, according to the robust geometric estimator design presented in Hernández and Alvarez (2003). This study with experimental testing established the feasibility of using a model-based observer to yield present estimates and time-ahead predictions of C-viscosity and acid conversion, and recommended the development of software sensors based on indirect C-viscosity measurements to improve the estimation-prediction scheme. On the other hand, the calorimetric estimation technique has been extensively and

successfully used to estimate and control variables in solution and emulsion polymer reactors (Sáenz de Buruaga *et al*., 2000; Othman *et al*., 2001; Zaldo *et al*. 2002 and references there in). In particular, Zaldo *et al*. (2002) estimated the heat generation rate and the heat exchange coefficient on the basis of temperature and flow measurements.

In this paper the problem of designing and experimentally testing a heat exchange devise to infer the C-viscosity and the acid conversion in an alkyd reactor is addressed. The underlying time-varying nonlinear observability property is identified, yielding the design of the heat exchange devise and the construction of the corresponding nonlinear observer with a robust convergence criterion coupled to a simple tuning scheme.

2. SOFTWARE SENSOR DESIGN PROBLEM

Consider the alkyd reactor presented in Figure 1, where fatty acids, polybasic acids, and polyols are terpolymerized via an endothermic polyesterification reaction. Since the polymerization reaction is endothermic, heat must be added to maintain a constant temperature (typically 240 °C), and water product must be removed to favor the reaction advance. In an industrial reactor, the monitoring of viscosity and acidity is periodically executed with a 30 to 60 minutes delay period between the sample acquisition and its analysis in the laboratory. These results in conjunction with a calibrated C-viscosity (referred to 25°C) versus acid group conversion chart are employed in an advisory type control scheme to decide on corrective additions of acid groups, to predict the gelation point of the cold product, and to decide the end of the batch. In principle, the overall reactor performance should benefit from the passage from this advisory control scheme towards one more systematic with continuous measurements or suitable estimates and with feedback control actions, and this is the motivation for the consideration of an on-line C-viscosimeter (Händel, 1996).

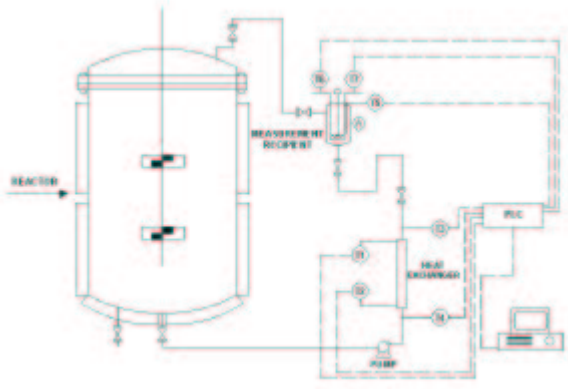

Figure. 1. Software sensor system

In this work, the main idea is the replacement of the aforementioned on-line viscosimeter by the heat exchange device (A) shown in Figure 1. The proposed hardware consists of a continuous sampling recirculation loop equipped with a heat exchanger to cool the resin down to a suitable temperature T_v and a stirred vessel with a cooling coil, so that the measured heat exchange rate

$$y = w_j\, c_{pj}\, (T_{ji} - T_{jo}) \tag{1}$$

reflects the C-viscosity of the resin in the vessel. w_j is the mass flow rate of cooling water, c_{pj} is its specific heat capacity, and T_{ji} (or T_{jo}) is its inlet (or outlet) temperature. From a steady-sate heat balance follows that the total heat exchange rate between the resin in the test vessel and its cooling coil is given by

$$Q = U(\mu, \mu_w)\, (\pi D_o\, L_c)\, \tau\, (T_v, T_{ji}, T_{jo}) \tag{2a}$$
$$:= \theta\, (c, T_v, T_{ji}, T_{jo}, p_\theta)$$

where D_o (or L_c) is the coil outside diameter (or length), τ is the log-mean temperature difference, and U is the global heat transfer coefficient (Oldshue, 1983):

$$U(\mu, \mu_w) = [1/h_r(\mu, \mu_w) + (r_2/r_1)\, (1/h_j)]^{-1} \tag{2b}$$

$$h_r(\mu, \mu_w) = a_h\, (k_r/D)\, [R_e(\mu)]^{b_h} [P_r(\mu)]^{c_h} [\mu/\mu_w]^{d_h} \tag{2c}$$

$$P_r(\mu) = (\mu c_{pr}/k_r), \qquad R_e(\mu) = (D^2 N \rho/\mu) \tag{2d}$$

$$\tau\,(T_v, T_{ji}, T_{jo}) = (T_{ji} - T_{jo})/\ln[(T_v - T_{ji})/(T_v - T_{jo})] \tag{2e}$$

$$T_j = T_v - \tau\,(T_v, T_{ji}, T_{jo}) := ?\,(T_v, T_{ji}, T_{jo}) \tag{2f}$$

$$T_w = T_j - Q/[h_j\, (\pi D_i\, L_c)] := \iota\,(T_v, T_{ji}, T_{jo}) \tag{2g}$$

$$p_\theta = [c_{pr}, c_{pj}, D_i, D_o, D, h_j, k_r, L_c, N, \rho, \rho_j\,]'$$

h_r is the resin heat transfer coefficient, h_j is the coil-fluid heat transfer coefficient, r_1 (or r_2) is the coil outside and inside radius, D is the vessel diameter, D_i is the coil inside diameter, k_r is the resin conductivity, T_j is the coil-fluid mean temperature, μ is the resin viscosity at the vessel temperature T_v, μ_w is the resin viscosity at the temperature T_w of coil wall, P_r is the Prandtl number, and R_e is the Reynolds number.

The resin viscosity depends on the temperature (T) and the acid conversion (c) via the free volume-type expression:

$$\mu = \exp\{a_\eta(T) + b_\eta(T)\, \ln[A_0(1\text{-}c)] \tag{3}$$
$$+ c_\eta(T)\, [\ln\,(A_0\,(1\text{-}c))]^{\,2}\} := \alpha(c, A_0, T, p_\eta),$$

$$c = 1\text{-}A/A_0, \qquad p_\eta = [a_\eta, b_\eta, c_\eta]'$$

A is the acid number (i.e., mg of KOH required to neutralize one g of resin), A_0 is its initial value, and c

is the related conversion. p_η is the parameter vector of the relationship viscosity-conversion.
Our hardware sensor problem consists in choosing the dimension, geometry, mixing pattern, stirring, and mass flow (w_r) of the stirred vessel as well as the material, diameter, length, and cooling fluid inlet temperature of the coil. Our software problem consists in designing a robust nonlinear observer that yields estimates of the C-viscosity (η) and of the conversion (c):

$$\eta = \alpha(c, A_0, T_v, p_\eta) \tag{4}$$

Methodologically speaking, we are interested in identifying a physically interpreting the nonlinear time-varying observability property that underlies the hardware and software designs of the finite-time batch alkyd polymer reactor.

3. ESTIMATION MODEL

Phenomenological second and third apparent-order models have been employed in alkyd kinetic studies (Flory, 1953; Lin and Hsieh, 1977; Aigbodion and Okieimen, 1996), and none of the existing models apply to the entire course of the reaction. Any of these models with an adjustable (i.e. observable) constant leads to a third order nonlinear estimator (López et. al. 2000). To reduce the model order by one, let us recall a well-known fact in alkyd kinetic studies and industrial reactor operation: at constant temperature, the C-viscosity increases exponentially with time. It means that, in C-viscosity coordinate Eq. (4), the third-order conversion model can be replaced by the following second-order model:

$$\dot\eta = k\,\eta, \qquad \eta(0) = \eta_0 \tag{5a}$$

$$\dot k = u_k(t) = v_k\,[\eta, A_0, T_v, \dot T_v, w, \dot w, p_\kappa] \approx 0, \tag{5b}$$

$$y = h(\eta, d, p), \qquad c = \beta(\eta, A_0, T_v, p_\eta) \tag{5c,d}$$

where w is a set of unmodeled variables related to the polymer molecular architecture, p_κ is a parameter vector associated to reaction rate, and β is the inverse map of the map α (Eq. 4) with respect to c. It is,

$$\beta[\alpha(c,A_0,T_v,p_\eta),T_v,p_\eta] = c \tag{6}$$

Finally, h is the heat rate exchange measurement map θ Eq. (2a) expressed in C-viscosity coordinate (η):

$$h(\eta, d, p) = \theta[\beta(\eta, A_0, T_v, p_\eta), T_{ji}, T_{jo}, p_\theta] \tag{7}$$

In vector notation, the estimation model (5) is given by

$$\dot x = f(x), \qquad x(0) = x_0,\ 0 \le t \le t_f \tag{8a}$$

$$y = H[x, d(t), p], \qquad c = B(x, p_\eta) \tag{8b}$$

where

$$x = (\eta, k)', \qquad d = [T_v, T_{ji}, T_{jo}]', \qquad p = [p_\theta, p_\eta]'$$

$$f(x) = (k\eta, 0)', \quad H[x, d(t), p] = h(\eta, d, p)$$

$$B(x, p_\eta) = \beta(\eta, A_0, T_v, p_\eta)$$

Since the maps f, H and B are continuously differentiable, a given data triplet $[x_0, d(t), p]$ uniquely determines a state motion x(t) and an output trajectory y(t):

$$x(t) = \tau_x[t, 0, x_0, d(t), p], \quad 0 \le t \le t_f \tag{9a}$$

$$y(t) = H[x(t), d(t), p] \tag{9b}$$

4. OBSERVABILITY PROPERTY

In this section is characterized the time-varying nonlinear observability property that underlies the solvability of the hardware and software design problems.

From the definition of nonlinear motion observability given in Alvarez and López, (1999) and Hernandez and Alvarez (2003), the observability property is defined for one particular finite-time motion x(t), or equivalently, for one particular input-output realization [y(t)-d(t)] of the batch reactor. The reactor motion x(t) is observable if at each time t, the state x(t) is uniquely determined by the measurement y(t) and its time derivative, or equivalently, if the state x(t) is the unique solution of the algebraic equation pair at time t:

$$y = h(\eta, d, p) := \phi_1(\eta, d, p), \quad \delta = (d, \dot d) \tag{10a}$$

$$\dot y = [\partial_\eta h(\eta, d, p)]k\eta + [\partial_d h(\eta, d, p)]\dot d := \phi_2(\eta, k, \delta, p) \tag{10b}$$

or

$$\psi = \phi(x, \delta, p), \quad \psi = (y, \dot y), \quad \phi = (\phi_1, \phi_2) \tag{10c}$$

From the local inverse theorem (Isidori, 1995), follows that this equation has a unique solution for x if the *nonlinear observability matrix*

$$O(x, \delta, p) = \partial_x \phi(x, \delta, p) = \begin{bmatrix} \partial_\eta h(\eta,d,p) & 0 \\ \sigma(x,d,p) & \eta\,\partial_\eta h(\eta,d,p) \end{bmatrix} \tag{11}$$

$$\sigma(x, d, p) = \partial_\eta \phi_2(\eta, k, \delta, p) = k[\eta\,\partial_{\eta\eta} h(\eta, d, p) +$$

$$\partial_\eta h(\eta, d, p)] + [\partial_{d\eta} h(\eta, d, p)]\,\dot{d}$$

is nonsingular along the reactor motion x(t). The determinant (det) and its (2-norm) minimum singular value (*msv*) s are given by

$$\det[O(\eta, d, p)] = \eta[\partial_\eta h(\eta, d, p)]^2$$
$$\text{msv}[O(\eta, d, p)] := s(\eta, d, p) = \partial_\eta h(\eta, d, p)$$

Thus, the motion x(t) is locally (nominally) observable if

$$\partial_\eta h[\eta(t), d(t), p] \neq 0 \quad \forall\, t \in [0, t_f]$$

Let X_0 and D are sets of perturbed initial and exogenous inputs about x(t) and d(t), respectively:

$$X_0 = \{\hat{x}_0 \mid |\hat{x}_0 - x_0| \leq \delta_0\}, \quad D = \{\hat{d}(t) \mid \|\hat{d}(t) - d(t)\| \leq \delta_d\}$$
$$\|\hat{d}(t) - d(t)\| = \max_{[t,\, t_f]} |\hat{d}(t) - d(t)|$$

where |x| is the norm of x, and δ_0 (or δ_d) is the radius of X_0 (or D). Let X be the corresponding bundle set o perturbed motions $[\hat{x}(t)]$ about x(t)

$$X = \{\hat{x}(t) = \tau_x[t, 0, \hat{x}_0, \hat{d}(\cdot), p], 0 \leq t \leq t_f \mid [\hat{x}_0, \hat{d}(t)]$$
$$\in X_0 \times D, \ \|\hat{x}(t) - x(t)\| \leq \varepsilon_x(\delta_0, \delta_d)\}, \ \varepsilon_x(0, 0) = 0$$

with $\varepsilon_x(\delta_o, \delta_d)$ being the radius of X. According to the definition of practical (i.e., no local) observability given in Alvarez *et al.* (2000), the (unperturbed) motion x(t), or equivalently, its uniquely associated input-output realization [d(t)-y(t)], is robustly observable for X (determined by X_0 xD) and a given lower bound s_* for the msv of the observability matrix if the following inequality is met

$$\partial_\eta h[\hat{\eta}(t), \hat{d}(t), p] > s_*\,, \ \forall\, [\hat{x}(t), d(t)] \in X \times D \qquad (12)$$

The fulfillment of this robust detectability property signifies that the reactor state motion x(t) can be robustly reconstructed via a nonlinear observer (Alvarez and López, 1999), with a measurement error (in y and h) propagation proportional to $1/s_*$.

Once the robust observability condition is met, the design of the corresponding geometric (i.e., Luenberguer-type) nonlinear observer follows from a straightforward construction-tuning scheme. This subject will be further discussed in subsection 5.3.

On physical grounds, the resin viscosity $\mu(c, T)$ decreases with temperature; the heat exchange rate h increases with temperature. The dependency ($\partial_\eta h$) of h on the C-viscosity (at T_v) η diminishes with the increase of the vessel temperature T_v, meaning that this temperature T_v must be set sufficiently low to yield an admissible sensitivity of the heat exchange rate with respect to acid conversion changes along the course of the reaction, or equivalently, to adequately meet the robust motion observability condition Eq. (12). On the other hand, the considerations of mixing and flow through pipe impose restrictions on the lowest resin temperature that can be reached in the sample vessel. Thus, the hardware design problem amounts to finding a vessel temperature T_v that represents a suitable compromise between the fulfillment of the robust observability condition Eq. (12) and the handling of a cold (i.e., viscous) resin fluid in the vessel and pipes of the sampling circulation loop. This subject on the hardware design will be discussed in subsection 5.1.

5. SOFTWARE SENSOR DESIGN

5.1. Experimental setting (Hardware design)

In order to calibrate the estimation model, an initial alkyd polymerization was carried out at 210 °C in an 80 L reactor with the system shown in Figure 1. The reactor was loaded with a mixture of fatty acids, phthalic anhydride, glycerine, and pentaerytritol. For industrial confidentiality reasons, the composition of initial load cannot be revealed. Following previous reports (Händel, 1996), the sample vessel temperature was set at T = 125 °C. At the reactor high temperature (210 °C), the term $\partial_\eta h$ in the observability condition Eq. (12) is very small, meaning that the model observability is very poor. Consequently, the resin temperature had to be decreased to increase the value of $\partial_\eta h$ and have adequate sensitivity. It was verified that the vessel temperature T_v = 125 °C was an adequate value to meet the robust observability condition with a manageable flowrate in the recirculation loop.

The kind of vessel stirrer and its revolutions per minute N, as well as the baffles were chosen according to standard design mixing equipment considerations (Oldshue, 1983), enhancing the macromixing for heat exchange purposes. The inlet coil water temperature was fixed at T_{ji} = 20 °C. The coil diameter was fixed at D_o, and an initial value for the jacket fluid flow-coil length pair $(w_j\text{-}L_c)_0$ was chosen according to the aforementioned heat transfer correlations, in the understanding that this pair will be adjusted in order to adequately meet the robust observability condition Eq. (12). The temperature of the vessel and the input and output temperatures of the coil were on line measured and the heat exchange rate was measured. Samples of the resin were taken from the reactor and off-line analyzed: the C-viscosity

is measured with an ICI cone-plate viscosimeter over the temperature range of [100, 150°C, i.e., bracketing the one of 125 °C reported by Händel (1996)], and the acid number was determined by KOH titration.

5.2. Model calibration

The C-viscosity at different temperatures and acid number measurements obtained from the samples were fed to a nonlinear regressor, yielding the coefficients of the free-volume type (Eq. 3) nonlinear map α (Eq. 4):

$$a_\eta(T) = 3477.99/(T + 273) - 3.1815$$
$$b_\eta(T) = -456.961/(T + 273) - 1.9603$$
$$c_\eta(T) = -185.203/(T + 273) + 1.1656$$

From the measured heat exchange values, the parameters of the heat exchange coefficient expression (Eq. 2c) were adjusted, obtaining the following results for this equation,

$$a_h = 1.178\ ,\ b_h = 2/3,\ c_h = 1/3\ ,\ d_h = 0.14$$

Finally, it was found that the agitation due to the recirculation loop amounted to an effective stirred speed (N) of 200 rpm (i.e. 30 rpm more than in the case without recirculation.)

5.3. Software design

Given the nonlinear nonsingular observability matrix (Eq. 11), and having designed the hardware so that the robust observability condition Eq. (12) is adequately met in the light of equipment specifications and restrictions, the construction of the corresponding geometric nonlinear observer follows from a straightforward application of the procedure given in Alvarez and López (1999):

$$\dot{\hat{x}} = f[\hat{x}, d(t), p_e] + G[\hat{x}, d(t), p_e]\{y - h[\hat{x}, d(t), p_e]\}$$
$$G(\hat{x}, d, p_e) = [O^{-1}(\hat{x}, \delta, p)]\, k_e(\zeta, \omega)'$$
$$k_e(\zeta, \omega) = (2\zeta\omega, \omega^2)$$

where G is a nonlinear gain matrix, ζ (or ω) is the damping (frequency) adjustable parameter of the output error response. The estimator converges if the celerity parameter is chosen so that the following inequality is met:

$$\omega > 2\zeta(\partial_\eta \phi_2)/(\partial_\eta h)$$

In detailed form, the estimator is given by

$$\dot{\hat{\eta}} = \hat{k}\hat{\eta} + g_\eta[\hat{\eta}, d(t), \zeta, \omega, p_e]\{y - h[\hat{\eta}, d(t), p_e]\} \quad (13a)$$

$$\dot{\hat{k}} = g_k[\hat{\eta}, d(t), \zeta, \omega, p_e]\{y - h[\hat{\eta}, d(t), p_e]\} \quad (13b)$$

$$\hat{c} = \beta(\hat{\eta}, A_0, T_v, p_\eta) \quad (13c)$$

where

$$g_\eta(\eta, d, \zeta, \omega, p_e) = 2\zeta\omega/[\partial_\eta h(\eta, d, \zeta, \omega, p_e)]$$
$$g_k(\eta, d, \zeta, \omega, p_e) \approx \omega^2/[\eta\partial_\eta h(\eta, d, \zeta, \omega, p_e)]$$

$$\zeta = 0.71, \qquad \omega = 10\,k^*, \qquad k^* \approx \partial \ln\eta/\partial t$$

k^* is a representative value of the viscosity dynamics, and the value of ω means that the observer is tuned about ten times faster than the C-viscosity dynamics. In our case ($k^* = 0.00324\ \text{min}^{-1}$) this tuning yielded an adequate compromise between reconstruction rate and tolerance to measurement and modeling errors.

6. EXPERIMENTAL IMPLEMENTATION

The proposed software sensor Eq. (13) was tested in the pilot plant system presented in Figure 1. In Figure 2 are shown the on-line estimated and off- line C-viscosity values. As it can be seen, the evolution of C-viscosity is reasonably followed and there is a good agreement between the on-line and off-line values. In Figure 3, the evolution of the estimated and measured heat exchange rate are presented. Finally, in Figure 4 are presented the on-line estimated and off-line (titration) measurements of acid number. As it can be seen in the figures, the software sensor provides reasonable estimates in the light of the modeling assumptions and uncertainties. It must be pointed out that the free-volume Eq. (3) and heat transfer (Eq. 2c) correlations should be occasionally calibrated, especially when a new formulation or raw material is to be polymerized.

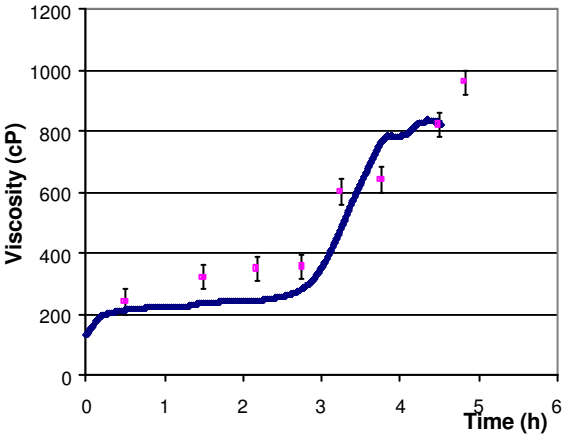

Figure 2. On-line (—) and off-line (¦) C-viscosity.

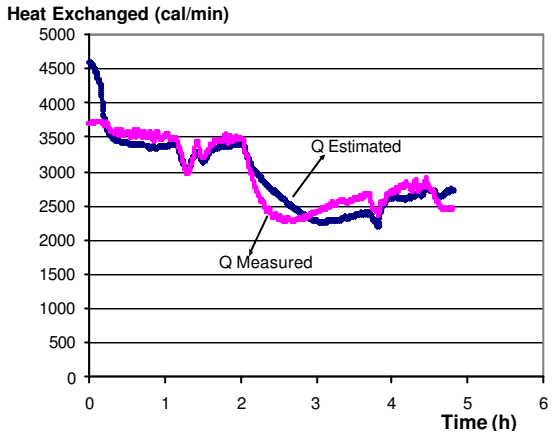

Figure 3. Estimated (—) and measured (¦) heat exchange rate.

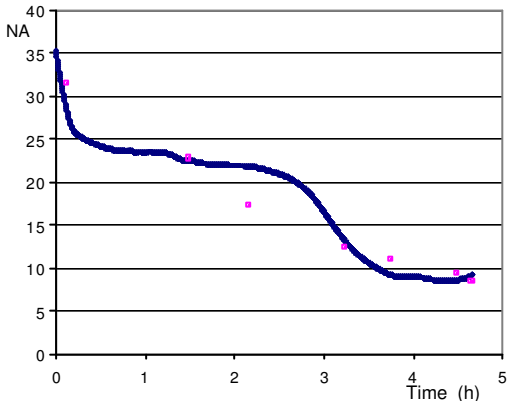

Figure 4. On-line (—) and off-line (¦) acid number.

7. CONCLUSIONS

In this work, a calorimetric software sensor to on-line estimate the cold viscosity and acid number of alkyd resins has been developed and implemented in a pilot plant. The experimental testing of the resulting software sensor shows the feasibility of drawing an on-line estimate of the cold viscosity and acid conversion based on the heat exchanged measurement. The characterization of the underlying nonlinear robust observability property enabled a unified approach to the hardware and software design aspects of the problem.

REFERENCES

Aigbodion, A.I., and F.E. Okieimen (1996). Kinetics of the preparation of rubber seed oil alkyds. *Eur. Polym. J.*, **32**(9), 1105.

Alvarez, J., and T. López (1999). Robust dynamic state estimation of nonlinear plants. *AIChE J.*, **45**(1), 107.

Alvarez, J., T. López, and E. Hernández (2000). Robust Estimation of Free-Radical Homopolymer Reactors. *Journal of Process Control*, **10**, 389.

Eliçabe, C.E. and G.R. Meira (1988). Estimation and control in polymerization reactors. *Polymer. Eng. and Sci.* **28**(3), 121.

Ellis, M.F., T.W. Taylor and K.F. Jensen (1994). On-line molecular weight distribution estimation and control in batch polymerization. *AIChEJ.* **40**(3), 445.

Flory, P.J. (1953). Principles of polymer chemistry. Cornell Univ. Press. New York.

Händel, E. (1996). Nicht nur einen Gang Gespart. FARBE &LACK 102, Jahrgang 11, 135. BASF Patent.

Hernández, H. and J. Alvarez (2003). Robust estimation of continuous nonlinear plants with discrete measurements. *Journal of Process Control,* **13**, 69.

Isidori, A. (1995). *Nonlinear control systems*, 3th Ed., Springer-Verlag, New York.

Lin, C.C., and K.H. Hsieh (1977). The kinetics of polyesterification. I. Adipic acid and ethylen glycol. *J. Appl. Polym. Sci.*, **21**, 2711.

López, T., H. Hernández, and J. Alvarez (2000). Robust nonlinear estimation of alkyd reactors with discrete-delayed measurements, *ADCHEM2000 Congress*, Pisa, Italy.

Mutha, R.J, W.R. Cluett and A. Penlidis (1997). On-line nonlinear model-based estimation and control of a polymer reactor. *AIChE J.* **43**(11), 3042.

Oldshue, J.Y. (1983). Fluid Mixing Technology. Chem. Eng. McGraw-Hill Publications Co., New York.

Othman, N., G. Fevotte, and T. F. McKenna (2001). On-line Monitoring of Emulsion Terpolymerization Processes. *Polym. React. Eng.*, **9**(4), 271

Patton, T.C. (1962). Alkyd resin technology. John Wiley & Sons. NY.

Sáenz de Buruaga, I., Leiza, J. R., and J. M. Asua, (2000). Model-based Control of Emulsion Terpolymers Based On Calorimetric Measurements. *Polym. React. Eng.*, **8**(1), 39.

Zaldo, F., Hernández, M., and J. Alvarez (2002). Calorimetric Estimation of Semibatch Emulsion Homopolymer Reactors. *Submitted to AIChE J*

STATE ESTIMATION IN BATCH CRYSTALLIZATION USING REDUCED POPULATION MODELS

S. Motz S. Mannal E.D. Gilles

Institut für Systemdynamik und Regelungstechnik,
Universität Stuttgart, Pfaffenwaldring 9, 70550 Stuttgart,
Germany

Abstract: This contribution deals with the design of an observer for state estimation of a batch crystallizer, which is described by a detailed population balance model. Therefore, the rigorous model containing (partial) integro-differential equations is first reduced by applying an integral approximation technique to a model of moments that consists of only a few ordinary differential equations. This reduced model serves then as the basis for the design of a Luenberger type observer. The performance of the observer is finally demonstrated by using the rigorous population balance model for the simulation of the crystallizer plant.

Keywords: state estimation, observer, population balance, model of moments, model reduction, integral approximation

1. INTRODUCTION

In a lot of crystalline product manufacturing applications the product quality is determined by the crystal size distribution. The main difficulty in batch production is thus to accomplish uniform and reproduceable particle size distributions. A suitable model based technique for monitoring each batch with respect to a reference batch is the state estimation by an observer (Ray 1981). Detailed descriptions of particulate processes are usually based on population balances, which generally leads to a complex mathematical model structure. An observer design based on such a population balance model is thus very difficult, if not impossible. Therefore, a model reduction technique will be applied in this contribution, which reduces the model formulation to a system of only a few ordinary differential equations. With the help of this reduced model it will then be possible to apply standard design techniques for a nonlinear observer (Schaffner and Zeitz 1995).
The paper is organized as follows: After a compendious description of the population balance model for the considered batch crystallizer, the applied model reduction technique, which is based on integral approximation, will be illustrated. An observer will then be designed based on the derived reduced model. Simulation results will finally illustrate the performance of the observer.

2. MODELING OF BATCH CRYSTALLIZERS

The batch cooling crystallizer considered in this contribution is a two phase system, which consists of a continuous liquid phase L and a dispersed solid phase S, see Fig. 1. The continuous liquid phase, which contains a binary mixture of *dissolved crystals* and *solvent*, is modeled by material balances. The population of individual crystals within the dispersed solid phase is described us-

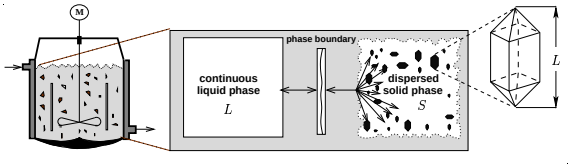

Fig. 1. Decomposition of a batch crystallizer.

ing the population balance approach (Ramkrishna 2000). In order to take the cooled operation of the batch crystallizer on different temperature levels into account, the model is completed by energy balances for the overall crystallizer content and for the coolant inside the cooling jacket.
In the following, the structure of the mathematical model for the considered crystallizer will be shortly described. For more details about the modeling of this type of crystallization processes, the reader is referred to (Gerstlauer *et al.* 2002).

2.1 Modeling of the dispersed solid phase

The application of the population balance approach in order to model the dispersed solid phase S leads to the following population balance equation for the number density function F depending on time t and the characteristic particle length L:

$$\frac{\partial F}{\partial t} = -\frac{\partial (G\,F)}{\partial L} + \dot{F}_{nu}^{+} + \dot{F}_{at}^{\pm} \qquad (1)$$

$$F(L, t=0) = F_{seed}(L)\,; \quad F(L=0, t) = 0\,.$$

The first term on the right hand side of Eq. (1) accounts for crystal growth with the growth rate G. The source due to nucleation is denoted by $\dot{F}_{nu}^{+}$. The term $\dot{F}_{at}^{\pm}$ summarizes all sinks and sources due to attrition of crystals at the stirrer. The initially added seed crystals are denoted by F_{seed}. All considered phenomena are described using detailed kinetic relations. The number of primary nuclei is calculated following Mersmann (1996), considering homogeneous and heterogeneous nucleation. The growth rate

$$\frac{G(\Delta c_{L,A}, L)}{2k_d(L)} = \frac{\Delta c_{L,A}}{c_S} + \frac{k_d(L)}{2k_r c_S} - \sqrt{\left(\frac{k_d(L)}{2k_r c_S}\right)^2 + \frac{k_d(L)}{k_r c_S}\frac{\Delta c_{L,A}}{c_S}} \qquad (2)$$

accounting for integration and diffusion limited crystal growth (Mersmann *et al.* 1992, Gahn and Mersmann 1999) depends on the supersaturation $\Delta c_{L,A}$ and on the size dependent mass transfer coefficient

$$k_d(L) = \frac{D_{AB}}{L}\left[0.8\left(\frac{\bar{\varepsilon} L^4}{\nu_L^3}\right)^{\frac{1}{5}}\left(\frac{\nu_L}{D_{AB}}\right)^{\frac{1}{3}} + 2\right], \qquad (3)$$

where D_{AB} is the diffusion coefficient and $\bar{\varepsilon}$ and ν_L denote the specific energy input and the kinematic viscosity. For the calculation of the attrition rate β and the number N_{frag} and size distribution f_{frag} of abraded fragments a very detailed model is used, which takes the stirrer geometry and the hardness of the crystalline material into account (Gahn and Mersmann 1999). In the population balance (1), this leads to a sink

$$\dot{F}_{at}^{-}(L) = \beta(L) F(L) \qquad (4)$$

due to the crystals that collided with the stirrer, to a source term $\dot{F}_{at,1}^{+}$ accounting for the resulting large crystal with a length $L' - \Delta L(L')$ somewhat smaller than the size L' of the original crystal and to a source term $\dot{F}_{at,2}^{+}$ for all produced fragments:

$$\dot{F}_{at,1}^{+} = \int_L^\infty \delta\left(L - (L' - \Delta L(L'))\right) \dot{F}_{at}^{-}(L')\, dL' \qquad (5)$$

$$\dot{F}_{at,2}^{+} = \int_L^\infty N_{frag}(L') f_{frag}(L, L') \dot{F}_{at}^{-}(L')\, dL'\,. \qquad (6)$$

2.2 Modeling of the continuous liquid phase

The continuous liquid phase L inside the crystallizer consists of two components: the solute and the solvent, i.e. component A and B, respectively. The fundamental balance equations for the liquid phase are thus a balance for the total number of moles n_L

$$\frac{dn_L}{dt} = (a+1)\cdot(-\dot{n}_{nu} - \dot{n}_{gr})\,, \qquad (7)$$

and a component mole balance for the number of moles $n_{L,A}$ of dissolved crystals (component A)

$$\frac{dn_{L,A}}{dt} = -\dot{n}_{nu} - \dot{n}_{gr}\,. \qquad (8)$$

Initial conditions for the balance equations (7) and (8) are given by

$$n_L(t=0) = n_{L,0} \text{ and } n_{L,A}(t=0) = n_{L,A,0}\,.$$

The variable a in Eq. (7) denotes the number of solvent molecules that form a crystal hydrate together with a single molecule of solute. The total molar fluxes $\dot{n}_{nu}$ and $\dot{n}_{gr}$ on the right hand sides of Eqs. (7) and (8) describe the exchange of material between the continuous liquid phase and the dispersed solid phase due to primary nucleation and crystal growth. With the nucleation rate B_{nu} and the growth rate G these molar fluxes are given by

$$\begin{aligned} \dot{n}_{nu} &= k_V \cdot c_S \cdot L_{crit}^3 \cdot B_{nu} \\ \dot{n}_{gr} &= k_V \cdot c_S \int_0^\infty L^3 \frac{\partial (G\,F)}{\partial L}\, dL\,. \end{aligned} \qquad (9)$$

The symbols k_V and c_S in Eqs. 9 denote the volume shape factor of the crystals and their molar density. The minimum size, which nuclei must have to be stable, is characterized by the critical crystal length L_{crit}.

2.3 Energy balances

Besides the population balance (1) and the material balances (7) and (8) energy balances accounting for the overall crystallizer temperature T_{cr} and for the temperatute T_j of the coolant inside the cooling jacket are required to complete the crystallizer model.
With the heat capacity $C_{P,cr}$ of the crystallizer content, the change of the crystallizer temperature with time is determined by

$$C_{P,cr}\frac{dT_{cr}}{dt} = -\Delta h^*_{cr}\,(\dot{n}_{nu}+\dot{n}_{gr}) + J_{cool} + W_{st} \qquad (10)$$

depending on the heat due to crystallization Δh^*_{cr}, the energy exchange J_{cool} with the cooling jacket and the energy dissipation W_{st} by the stirrer. In a similar way, the change of the temperature T_j inside the cooling jacket is given with the heat capacity $C_{P,j}$ of the coolant as

$$C_{P,j}\frac{dT_j}{dt} = c^*_{P,j,in}\dot{n}_{cool}\,(T_{j,in}-T_j) - J_{cool}. \qquad (11)$$

In this equation, the symbol $c^*_{P,j,in}$ denotes the molar heat capacity of the inflowing coolant $\dot{n}_{cool}$ and $T_{j,in}$ is the temperature of the inflowing coolant, which is the only manipulating variable to operate the process. Initial conditions for the energy balances (10) and (11) are given by

$$T_{cr}(t=0) = T_{cr,0} \text{ and } T_j(t=0) = T_{j,0}\,.$$

This concludes the description of the rigorous crystallizer model, which is made up of a partial integro-differential equation (1) for $F(L,t)$ and of four ordinary integro-differential equations (7), (8), (10) and (11) for $n_L(t)$, $n_{L,A}(t)$, $T_{cr}(t)$ and $T_j(t)$. This rigorous model will be the starting point for the following model reduction, and it will be used to validate the subsequently designed observer.

3. MODEL REDUCTION

With the model reduction technique described in this section, the infinite dimensional population balance (1) can be reduced to a set of six ordinary differential equations for the lower order moments

$$\mu_k(t) = \int_0^\infty L^k\,F(L,t)\,dL \quad k=0,\ldots,5 \qquad (12)$$

of the crystal size distribution $F(L,t)$. From a process engineering point of view, this reduction is not really a restriction, since the knowledge of the lower order moments is sufficient for most practical applications, but the great advantage of the resulting reduced model of moments is its model structure, which finally consists of only ten ordinary differential equations.
Such a moment based model reduction has already been applied by Hulburt and Katz (1964), but as mentioned by many authors, the analytical derivation of the moment equations

$$\frac{d\mu_k}{dt} = \int_0^\infty L^k\left(-\frac{\partial\,(GF)}{\partial L} + \dot{F}^+_{nu} + \dot{F}^\pm_{at}\right)dL\,, \qquad (13)$$

which can be derived by differentiating Eq. (12) with respect to time t, leads in general to an unclosed set of ordinary differential equations. In contrast to the analytical derivation (Hulburt and Katz 1964), in this contribution a numerical integral approximation, which is based on Gaussian quadrature rule (McGraw 1997), will be applied to evaluate the integral on the right hand side of Eq. (13). To illustrate this technique, the approximation of the k$^{\text{th}}$ moment yields for example

$$\mu_k(t) = \int_0^\infty L^k\,F(L,t)\,dL \simeq \sum_{i=1}^{n} L_i^k(t)\,w_i(t), \qquad (14)$$

where L_i amd w_i are so called abscissas and weights (Lanczos 1956). Since the sum on the right hand side of Eq. (14) results in the exact value of the integral for $k \le 2n-1$, the time dependent abscissas $L_i(t)$ and weights $w_i(t)$ can be calculated from

$$\begin{aligned} w_1 + w_2 + \ldots + w_n &= \mu_0 \\ L_1w_1 + L_2w_2 + \ldots + L_nw_n &= \mu_1 \\ L_1^2w_1 + L_2^2w_2 + \ldots + L_n^2w_n &= \mu_2 \\ \vdots \qquad\qquad\qquad & \quad \vdots \\ L_1^{2n-1}w_1 + \ldots + L_n^{2n-1}w_n &= \mu_{2n-1}\,. \end{aligned} \qquad (15)$$

For the solution of this *problem of weighted moments* (Lanczos 1956), several methods have been reported, see e.g. (Sack and Donovan 1972). All these methods are based on the fact that the abscissas L_i for the Gaussian quadrature rule can be determined as the zeros of orthogonal polynomials, which can be computed as the eigenvalues $[L_i\boldsymbol{I}-\boldsymbol{J}]=0$ of a tridiagonal matrix

$$\boldsymbol{J} = \begin{pmatrix} \beta_0 & \alpha_0 & 0 \\ \alpha_0 & \beta_1 & \alpha_1 \\ 0 & \alpha_1 & \beta_2 \end{pmatrix} \qquad (16)$$

of size $n\times n$ (3×3 for $k=0,\ldots,5$), where α_i and β_i depend on the moments μ_k. The weights w_i can finally be obtained from the first components of the corresponding eigenvectors v_i

$$w_i = \mu_0 v_i(1)^2 \,. \tag{17}$$

Using the abscissas L_i and the weights w_i, the integrals on the right hand side of Eq. (13) and in Eqs. (9) can thus be approximated by applying

$$\int_0^\infty L^k \, \Phi(\underset{n}{L}) \, F(L,t) \, dL \approx \sum_{i=1} L_i^k(t) \, \Phi(L_i(t)) \, w_i(t) \tag{18}$$

with $\Phi(L)$ being any sufficiently smooth (kinetic) expression.
The application of this model reduction technique leads thus to a reduced model of moments that contains the material balances (7) and (8), the energy balances (10) and (11) and six ordinary differential equations for the first six moments $\mu_0, \ldots, \mu_5$ instead of the population balance (1). The resulting model can thus be formulated as

$$\begin{aligned} \dot{\boldsymbol{x}} &= \boldsymbol{f}(\boldsymbol{x}) + \boldsymbol{g}(\boldsymbol{u}) \,; \;\; \boldsymbol{x}(t=0) = \boldsymbol{x}_0 \\ \boldsymbol{y} &= \boldsymbol{h}(\boldsymbol{x}) \end{aligned} \tag{19}$$

with the state vector,

$$\boldsymbol{x} = \left(n_L \;\; n_{L,A} \;\; T_{cr} \;\; T_j \;\; \mu_0 \;\; \mu_1 \;\; \mu_2 \;\; \mu_3 \;\; \mu_4 \;\; \mu_5 \right)^T, \tag{20}$$

the output vector $\boldsymbol{y}$ and the control vector $\boldsymbol{u}$, which in case of this batch crystallizer only contains the temperature $T_{j,in}$ of the inflowing coolant. This form allows the derivation of a standard Luenberger type observer design (see e.g. in (Schaffner and Zeitz 1995)), which will be subject of the next section.

4. OBSERVER DESIGN

For state estimation, either for process monitoring tasks or with the objective of process control, the entire state of the batch crystallizer in terms of the number of moles n_L and $n_{L,A}$, the temperatures T_{cr} and T_j and the moments $\mu_0 - \mu_5$ of the crystal size distribution has to be reconstructed from available measurements. Nowadays, very efficient sensors are available for temperature measurement, as well as for the online determination of supersaturation, see e.g. the crystallizer setups described in (Miller 1993, Neumann 2001). Besides these sensors, also techniques are available for determining particle size distributions, e.g. from light scattering (MALVERN) or from chord length (LASENTEC) measurements. However, a drawback of these methods is that they work quite well, if additional information about the shape of the crystal size distribution is available, e.g. to calculate the size distribution from a chord length distribution (Ruf *et al.* 2000). But from these measurements values for certain moments can be derived, as e.g. μ_1 from the LASENTEC FBRM (Ruf *et al.* 2000) or μ_2 from the application of the MALVERN sensor (Miller 1993). Therefore, the following approach for an observer design will be based on the availability of either the first moment μ_1 or the second moment μ_2.
In case of the here considered batch crystallizer, the measured supersaturation, which is equivalent with the knowledge of the mole fraction $x_{L,A} = n_{L,A}/nL$, leads directly to the determination of the model states n_L and $n_{L,A}$, since the overall content of material keeps constant throughout the batch time. Moreover, the knowledge of $x_{L,A}$ allows the calculation of the third moment μ_3 using

$$\mu_3 = \frac{1}{k_V c_S} \left[n_{seed} + \frac{1}{1-(1+a)x_{L,A}} \left(n_{L,A,0} - x_{L,A} n_{L,0} \right) \right], \tag{21}$$

with n_{seed} being the number of moles of the seed crystals F_{seed}.
Thus, an output vector $\boldsymbol{y}$ can be defined containing six state variables, which are measured or directly related to measurements

$$\boldsymbol{y} = \left(n_L \;\; n_{L,A} \;\; T_{cr} \;\; T_j \;\; \mu_* \;\; \mu_3 \right)^T \tag{22}$$

with μ_* defining either μ_1 or μ_2. Based on this output vector $\boldsymbol{y}$, a Luenberger type observer (Schaffner and Zeitz 1995) of the form

$$\begin{aligned} \dot{\hat{\boldsymbol{x}}} &= \boldsymbol{f}(\hat{\boldsymbol{x}}) + \boldsymbol{g}(\boldsymbol{u}) + \boldsymbol{L}(\boldsymbol{y} - \hat{\boldsymbol{y}}); \;\; \hat{\boldsymbol{x}}(t=0) = \hat{\boldsymbol{x}}_0 \\ \hat{\boldsymbol{y}} &= \boldsymbol{h}(\hat{\boldsymbol{x}}) \end{aligned} \tag{23}$$

can be established. Here, $\hat{\boldsymbol{x}}$ represents the vector containing the estimated states, $\boldsymbol{f}(\hat{\boldsymbol{x}}) + \boldsymbol{g}(\boldsymbol{u})$ is a copy of the right hand sides of the reduced model, $\boldsymbol{L_{obs}}(\boldsymbol{y} - \hat{\boldsymbol{y}})$ the correction term, and $\hat{\boldsymbol{y}}(\hat{\boldsymbol{x}})$ represents the estimator output vector. The initial values $\hat{\boldsymbol{x}}_0$ for the observer states are given by the initial states $\boldsymbol{x}_0$ of the reduced model of moments, which can be calculated from the initial conditions of the original rigorous population balance model.
For convergence of the estimated states $\hat{\boldsymbol{x}}$ against the states of the plant, the difference $\boldsymbol{y} - \hat{\boldsymbol{y}}$ has to converge to zero. In order to obtain this, a matrix $\boldsymbol{L_{obs}}$ has to be designed. Since the reduced model of moments has due to the involved eigenvalue problem a very complex nonlinear structure, it is not possible to determine $\boldsymbol{L_{obs}}$ by an analytical design method. But from physical considerations the structure of the matrix $\boldsymbol{L_{obs}}$ can be identified for the here considered batch crystallizer as

$$\boldsymbol{L_{obs}} = \begin{pmatrix} X_1^1 & 0 & 0 & 0 & 0 & 0 & 0 & 0 & 0 & 0 \\ 0 & X_2^2 & 0 & 0 & 0 & 0 & 0 & 0 & 0 & 0 \\ 0 & 0 & X_3^3 & 0 & 0 & 0 & 0 & 0 & 0 & 0 \\ 0 & 0 & 0 & X_4^4 & 0 & 0 & 0 & 0 & 0 & 0 \\ 0 & 0 & 0 & 0 & X_5^5 & X_5^6 & X_5^7 & 0 & 0 & 0 \\ 0 & 0 & 0 & 0 & 0 & 0 & 0 & X_6^8 & X_6^9 & X_6^{10} \end{pmatrix}^T . \tag{24}$$

All the entries $X_{i,j}$ represent adequate gain values, depending on the availability of μ_1 or μ_2. These gain values can be adjusted as constant values following again physical considerations. With this gain matrix $\boldsymbol{L_{obs}}$, the lower order moments $\mu_0 - \mu_2$ are adjusted with the measured μ_1 or μ_2, the higher order moments $\mu_3 - \mu_5$ by μ_3. Due to the ratio between the moments, this leads to typical gain values of e.g. $X_6^8 = 1 \cdot 10^{-2}$ and $X_6^9 = 1.84 \cdot 10^{-6}$.

As another consequence of the complex nonlinear system used for the observer design, it is not possible to investigate stability properties analytically. Therefore, simulation studies for different disturbed and undisturbed operation modes have to be carried out, in order to verify the applicability of the designed observer.

5. SIMULATION RESULTS

In this section, simulation results will be presented, in order to demonstrate the performance of the observer designed on the basis of the reduced model of moments. Therefore, the crystallizer setup by Miller (1993) will be considered, for which the detailed population balance model has already been validated (Gerstlauer *et al.* 2002). In this setup, a commonly used linear cooling regime for $T_{j,in}(t)$ is applied, as depicted in Fig. 2. All the following investigations are performed by

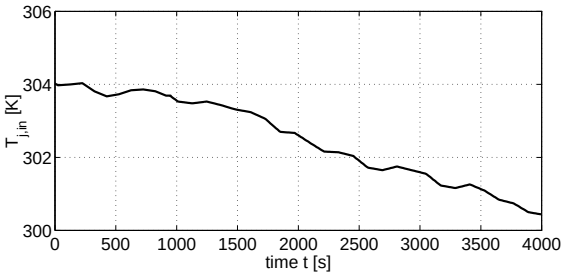

Fig. 2. The applied, approximately linear cooling rate in the crystallizer setup by Miller (1993).

using the rigorous population balance model for the simulation of the batch plant. The population balance is therefore discretized by a Method of Lines approach (Schiesser 1991) using 1000 grid points. For all simulations $10g$ of normally distributed seed crystals (mean: $500\mu m$; deviation $50\mu m$) are used. Both the plant model as well as the observer are solved using a standard ODE solver in MatLab [1] .

The robustness and performance of the observer based on the reduced model of moments and described in Eqs. (23) and (24) will in the following be analyzed by adding disturbances to the programmed cooling profile in Fig. 2. Therefore, the considered batch process will be simulated under rather heavily disturbed cooling profiles as can be seen in Fig. 3. For the further investigation

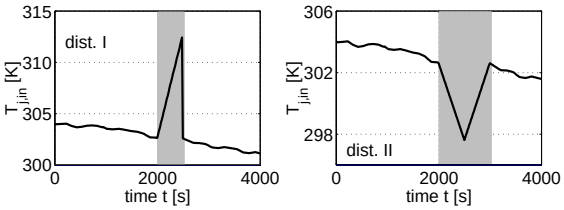

Fig. 3. Applied disturbed cooling profiles.

of the observer behavior, two state estimators will be used, one for the availability of μ_1 and another for the measurement of μ_2. In the following comparisons between the estimated observer states with the states of the rigorous plant model, only those states will be discussed, for which no measurements are available.

In the first case, an observer based on the availability of μ_1 is considered. As can be seen in Fig. 4, this observer achieves very good results for an undisturbed operation of the batch crystallizer as well as for a disturbed cooling profile ('dist I' in Fig. 3). Fig. 4 shows clearly the significant

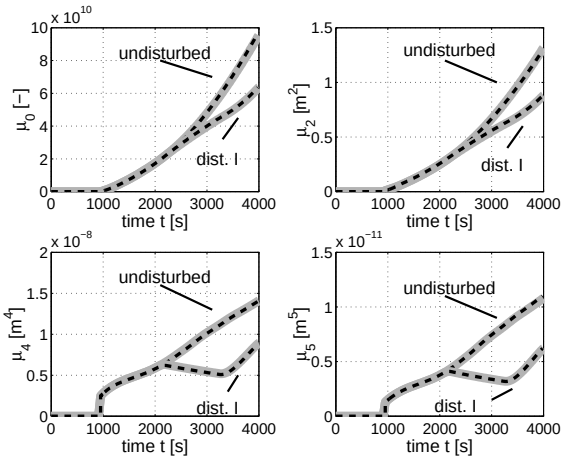

Fig. 4. Comparison of estimated moments μ_0, μ_2, μ_4 and μ_5 (dashed black lines) with the moment values calculated from the rigorous plant model (thick grey lines) for an observer based on the availability of μ_1.

consequences of the applied disturbance. The estimated states (dashed black lines) follow the plant states (thick grey lines) very well, even after the disturbance occured.

The observer considered in the second case, which is based on the availability of μ_2 has some more difficulties to follow the rigorous plant model, as can be seen in Fig. 5. As a consequence of disturbance II the estimated moments μ_0 and μ_1 start slightly drifting away from the plant states at about $2500s$, but due to the correction term $\boldsymbol{L_{obs}}(\boldsymbol{y} - \hat{\boldsymbol{y}})$ in Eq. (23) both μ_0 and μ_1 converge again and reach the plant states again after $3000s$.

[1] MatLab 5.3, The MathWorks Inc., 3 Apple Hill Drive, Natick, MA 01760-2098, USA

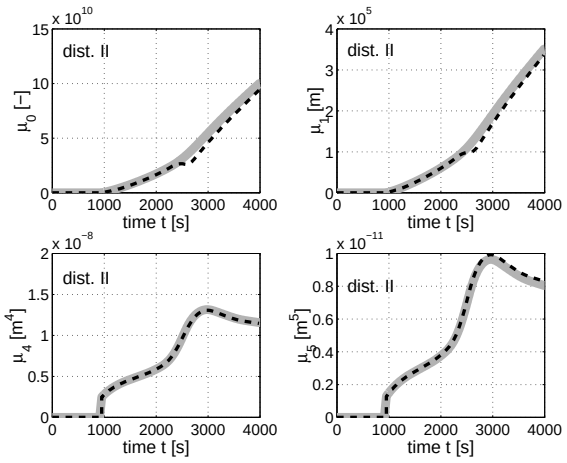

Fig. 5. Comparison of estimated moments μ_0, μ_1, μ_4 and μ_5 (dashed black lines) with the moment values calculated from the rigorous plant model (thick grey lines) for an observer based on the availability of μ_2.

The higher moments μ_4 and μ_5 are in perfect accordance during the whole process.
As depicted in Figs. 4 and 5 observers can be designed that achieve quite good results for both cases, the availability of μ_1 or μ_2.

6. SUMMARY AND CONCLUSIONS

In this contribution, an observer is designed for the state estimation of a batch crystallizer. The rigorous population balance model that describes this crystallization plant consists of (partial) integro-differential equations (Gerstlauer *et al.* 2002). After applying a model reduction technique, which is based on integral approximation using Gaussian quadrature rule (McGraw 1997), this infinite dimensional model can be reduced to a finite dimensional model that consists of only ten ordinary differential equations. On the basis of this reduced model of moments standard Luenberger type observers (Schaffner and Zeitz 1995) can be constructed, based on the availability of measurements of the first or the second moment of the crystal size distribution. As a consequence of the complex nonlinear design model, these observers are designed and tuned on the basis of process knowledge and physical considerations.
In the finally presented results, the rigorous population balance model is used to simulate the undisturbed and disturbed operation of the considered batch crystallizer. For all performed simulation studies, both observers behave very well, which demonstrates the applicability of these observers either for process monitoring or for the objective of process control.

ACKNOWLEDGEMENTS

The research project is supported within Sonderforschungsbereich 412 by Deutsche Forschungsgemeinschaft (DFG).

REFERENCES

Gahn, C. and A. Mersmann (1999). Brittle fracture in crystallization processes - Part A. and Part B.. *Chemical Engineering Science* **54**, 1273 – 1292.

Gerstlauer, A., S. Motz, A. Mitrović and E.D. Gilles (2002). Development, analysis and simulation of population models for industrial crystallizers. *Chemical Engineering Science* **57**(20), 4311 – 4327.

Hulburt, H. M. and S. Katz (1964). Some problems in particle technology - A statistical mechanical formulation. *Chemical Engineering Science* **19**, 555 – 574.

Lanczos, C. (1956). *Applied Analysis.* Prentice Hall.

McGraw, R. (1997). Description of Aerosol Dynamics by the Quadrature Method of Moments. *Aerosol Science and Technology* **27**, 255 – 265.

Mersmann, A. (1996). Supersaturation and nucleation. *Trans IChemE* **74**, 812 – 820. Part A.

Mersmann, A., M. Angerhöfer, T. Gutwald, R. Sangl and S. Wang (1992). General prediction of median crystal sizes. *Sep. Technol.* **2**, 85 – 97.

Miller, S. M. (1993). Modelling and Quality Control Strategies for Batch Cooling Crystallizers. PhD thesis. University of Texas at Austin.

Neumann, A. M. (2001). Characterizing Industrial Crystallizers of Different Scale and Type. PhD thesis. TU Delft.

Ramkrishna, D. (2000). *Population balances, theory and application to particulate systems in engineering.* Academic Press.

Ray, W. H. (1981). *Advanced Process Control.* McGraw-Hill.

Ruf, A., J. Worlitschek and M. Mazzotti (2000). Modeling and Experimental Analysis of PSD Measurements through FBRM. *Part. Part. Syst. Charact.* **17**, 167 – 179.

Sack, R. A. and A. F. Donovan (1972). An algorithm for Gaussian quadrature given modified moments. *Numer. Math.* **18**, 465 – 478.

Schaffner, J. and M. Zeitz (1995). Entwurf nichtlinearer Beobachter. In: *Entwurf nichtlinearer Regelungen* (S. Engell, Ed.). Oldenburg.

Schiesser, W. E. (1991). *The numerical method of lines - Integration of partial differential equations.* Academic Press.